Pharmacological blocking of microfibrillar-associated protein 4 reduces retinal neoangiogenesis and vascular leakage

Schlosser, Anders; Pilecki, Bartosz; Allen, Claire; Benest, Andrew V; Lynch, Amy P; Hua, Jing; Ved, Nikita; Blackley, Zoe; Andersen, Thomas L; Hennig, Dorle; Graversen, Jonas H; Möller, Sören; Skallerup, Sofie; Ormhøj, Maria; Lange, Clemens; Agostini, Hansjürgen T; Grauslund, Jakob; Heegaard, Steffen; Dacheva, Ivanka; Koss, Michael; Hu, Wenzheng; Iglesias, Bibiana; Lawrence, Matthew S; Beck, Hans Christian; Steffensen, Lasse Bach; Laursen, Nick S; Andersen, Gregers R; Holmskov, Uffe; Bates, David O; Sorensen, Grith L

Published in:
Molecular Therapy

DOI:
10.1016/j.ymthe.2025.01.038

Publication date:
2025

Document version:
Final published version

Molecular Therapy
Original Article

Pharmacological blocking of microfibrillar-associated protein 4 reduces retinal neoangiogenesis and vascular leakage

Anders Schlosser,[1] Bartosz Pilecki,[1] Claire Allen,[2] Andrew V. Benest,[2] Amy P. Lynch,[2] Jing Hua,[2] Nikita Ved,[2] Zoe Blackley,[2] Thomas L. Andersen,[3,4,5] Dorle Hennig,[1] Jonas H. Graversen,[1] Sören Möller,[6] Sofie Skallerup,[1] Maria Ormhøj,[1] Clemens Lange,[7,8] Hansjürgen T. Agostini,[8] Jakob Grauslund,[9] Steffen Heegaard,[10,11] Ivanka Dacheva,[12] Michael Koss,[12] Wenzheng Hu,[13] Bibiana Iglesias,[13] Matthew S. Lawrence,[13] Hans Christian Beck,[14] Lasse Bach Steffensen,[1] Nick S. Laursen,[15] Gregers R. Andersen,[15] Uffe Holmskov,[1] David O. Bates,[2] and Grith L. Sorensen[1]

[1]Department of Molecular Medicine, University of Southern Denmark, 5230 Odense, Denmark; [2]Cancer Biology, Division of Cancer and Stem Cells, School of Medicine, Biodiscovery Institute, University of Nottingham, Nottingham NG7 2UH, UK; [3]Molecular Bone Histology Laboratory, Department of Pathology, Odense University Hospital, 5000 Odense, Denmark; [4]Molecular Bone Histology Laboratory, Research Unit of Pathology, Department of Clinical Research, University of Southern Denmark, 5230 Odense, Denmark; [5]Danish Spatial Imaging Consortium (DanSIC), University of Southern Denmark, 5230 Odense, Denmark; [6]OPEN - Open Patient Data Explorative Network, Odense University Hospital and Department of Clinical Research, University of Southern Denmark, 5000 Odense, Denmark; [7]Ophtha-Lab, Department of Ophthalmology, St. Franziskus Hospital, 48145 Münster, Germany; [8]Eye Center, Medical Center, Faculty of Medicine, University of Freiburg, 79106 Freiburg, Germany; [9]Department of Ophthalmology, Odense University Hospital, 5000 Odense, Denmark; [10]Department of Pathology, Rigshospitalet, University of Copenhagen, 2100 Copenhagen, Denmark; [11]Department of Ophthalmology, Rigshospitalet-Glostrup, University of Copenhagen, 2600 Glostrup, Denmark; [12]Department of Ophthalmology, University of Heidelberg, 69047 Heidelberg, Germany; [13]Virscio, Inc., 5 Science Park, New Haven, CT 06511, USA; [14]Department of Clinical Biochemistry, Odense University Hospital, 5000 Odense, Denmark; [15]Department of Molecular Biology and Genetics, Aarhus University, 8000 Aarhus, Denmark

Neovascular age-related macular degeneration and diabetic macular edema are leading causes of vision loss evoked by retinal neovascularization and vascular leakage. The glycoprotein microfibrillar-associated protein 4 (MFAP4) is an integrin $\alpha_V\beta_{3/5/6}$ ligand present in the extracellular matrix. Single-cell transcriptomics reveal MFAP4 expression in cell types in close proximity to vascular endothelial cells, including choroidal vascular mural cells, retinal astrocytes, and Müller cells. Binding of the anti-MFAP4 antibody, hAS0326, makes MFAP4 inaccessible for integrin receptor interaction, and thereby hAS0326 blocked endothelial cell motility *in vitro*. Intravitreal hAS0326 inhibited retinal vascular lesion area and neovessel volume in a laser-induced choroidal neovascularization mouse model, vascular permeability in streptozotocin-induced retinopathy, and vascular leakage area in a chronic non-human primate model of DL-2-aminoadipic acid-induced retinopathy. One dose of hAS0326 showed duration of efficacy of at least 12 weeks in the latter model. Moreover, hAS0326 treatment significantly enriched Gene Ontology terms involving reduction of integrin binding. Our data suggest that hAS0326 constitutes a promising treatment of neovascularization and vascular leakage in retinal diseases.

INTRODUCTION

Neovascular age-related macular degeneration (nAMD) and diabetic macular edema (DME) are ophthalmic conditions caused by destabilization of the vasculature in the eye. nAMD and DME are leading causes of vision loss and blindness in the elderly and working-age populations, respectively. The prevalence of nAMD is >11% in persons aged ≥85 years.[1] More than 400 million people worldwide have diabetes,[2] 10% of whom show vision-threatening stages of diabetic retinopathy (DR) including DME.[3] Overexpression of vascular endothelial growth factor (VEGF), originally known as vascular permeability factor, plays an important role in the pathogenesis of vascular leakage, a critical hallmark of these diseases. Since the introduction of anti-VEGF therapy, intravitreal (i.v.t.) injections with anti-VEGF agents have become standard care and are often effective treatments for nAMD and DME. Despite continuous anti-VEGF treatment, significant visual loss occurs in about 23% of nAMD patients over 10 years[4] and identification of new treatment targets in retinal disease is warranted.

Integrins $\alpha_V\beta_3$ and $\alpha_V\beta_5$ have been shown to be highly induced by and to aggravate multiple pathological processes, such as vascular leakage, angiogenesis, and inflammation with relevance for retinal

Received 23 August 2024; accepted 22 January 2025;
https://doi.org/10.1016/j.ymthe.2025.01.038.

Correspondence: Grith L. Sorensen, Department of Molecular Medicine, University of Southern Denmark, 5230 Odense, Denmark.
E-mail: glsorensen@health.sdu.dk

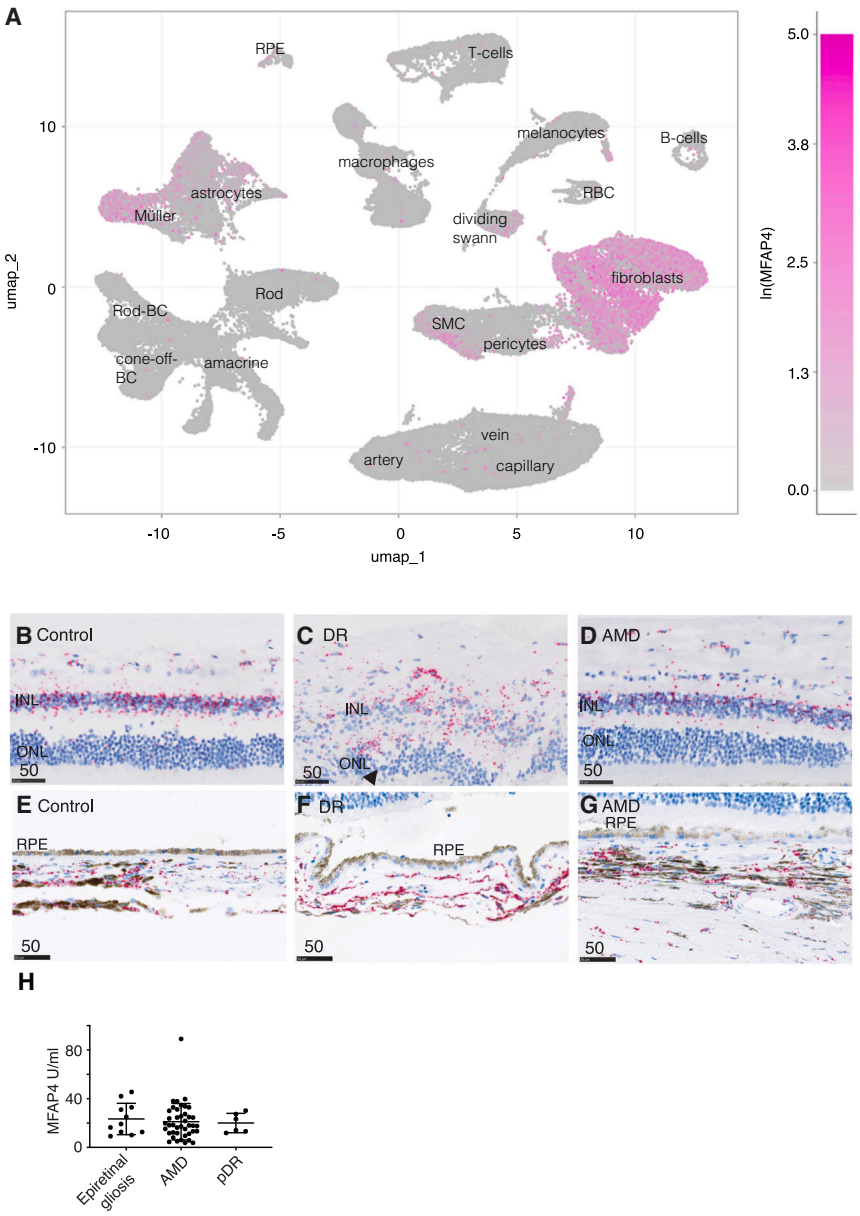

Figure 1. MFAP4 expression in the human eye

(A) Expression of *MFAP4* on Uniform Manifold Approximation and Projection (UMAP) from single-cell RNA sequencing analysis of ocular cells across human retina, RPE cells, and choroid. *MFAP4* mRNA *in situ* hybridization (punctate pink staining) of human (B) control retina, (C) diabetic retinopathy (DR) retina (with distorted morphology), (D) AMD retina, (E) control choroid, (F) DR choroid, and (G) AMD choroid. INL, inner nuclear layer; ONL, outer nuclear layer; RPE, retinal pigment epithelium. Scale bars are in μm. (H) Relative vitreous MFAP4 levels in patients: nAMD (AMD), age-related macular degeneration; pDR, proliferative diabetic retinopathy. Individual measurements are shown with means (SD). Groups were compared using one-way ANOVA followed by Tukey's multiple comparisons test.

diseases.[5] Proliferating endothelial cells express increased integrin levels,[6] while neutralization of integrin $\alpha_V\beta_3$ attenuates VEGF expression[7] and reduces the phosphorylation of its receptor VEGF-2.[8] Especially the role of the cellular integrin receptor $\alpha_v\beta_3$ in retinal disease is well described.[6] On this basis, integrins have gained interest as possible targets for therapeutic intervention in retinal disease[5] and trials are ongoing. However, the direct inhibition of α_V-integrins has historically been challenging. In the present study, we set out to test whether inhibition of an extracellular matrix (ECM) molecule microfibrillar-associated protein 4 (MFAP4), which is upstream of integrin activation, could serve as a potential treatment strategy in retinal diseases.

MFAP4 is a glycoprotein with elastin- and collagen-binding properties[9] and contains a tripeptide RGD motif with recognized cell interactions through integrin $\alpha_v\beta_3$ and $\alpha_v\beta_5$.[10,11] The reason for choosing MFAP4 as potential target is the protein's predominant expression in the vasculature relative to other organs.[12] This sets MFAP4 aside from most other integrin $\alpha_V\beta_3$ ligands and suggests a critical role for MFAP4 in the vasculature. MFAP4 appears to be involved in various vascular conditions as MFAP4-deficient mice are protected from arterial stenosis,[10] abdominal aortic aneurysm formation,[13] and hypertension.[14]

In this study, we developed a high-affinity monoclonal anti-MFAP4 antibody, hAS0326, with ability to efficiently block the MFAP4-integrin interaction. We use a multi-disciplinary array of experiments, including *MFAP4* expressional analysis of clinical samples, crystallography and biophysical experiments, *in vitro* studies, mouse and non-human-primate studies *in vivo*, and proteome analysis to support a role for MFAP4 and the neutralizing of MFAP4 as a treatment strategy in retinal disease.

RESULTS

MFAP4 expression in human retina and choroid

Single-cell transcriptional analysis across retina and choroid showed that *MFAP4* expression was predominantly observed in fibroblasts, smooth muscle cells (SMCs), pericytes, dividing Schwann cells, astrocytes, and Müller cells. Heatmap of MFAP4 expression is shown in Figure 1A and the corresponding dimensionality reduction is shown in Figure S1.

In situ hybridization analysis of *MFAP4* mRNA synthesis confirmed presence in the retina in controls, age-related macular degeneration (AMD) and DR. AMD samples showed histological presence of serous subretinal neovascular membrane and/or a subretinal hemorrhage. Patients with DR all had a diabetes duration >10 years, all had received laser photocoagulation, and were diagnosed with proliferative DR. MFAP4 mRNA expression was detected especially at the level of the inner nuclear layer where nuclei of Müller cells are located (Figures 1B–1D). Highly scattered expression was observed in areas of disease-induced distortion (Figure 1C). In support of the transcriptome analysis showing vascular expression (in SMCs and pericytes), *MFAP4* mRNA was also detected in the choroid (Figures 1E–1G) for all investigated eyes. Negative control for *in situ* hybridization is shown in Figure S2. These analyses did not allow quantification of MFAP4 expression. To analyze ocular protein levels, MFAP4 protein was measured in the vitreous of patients with epiretinal fibrosis, nAMD, and proliferative DR. Patient characteristics are shown in Table S1. Vitreous humor MFAP4 did not differ significantly between the studied ocular diagnoses. The combined analyses indicated that MFAP4 has a relatively high basal expression in the eye. Western blotting confirmed that intact MFAP4 protein was present in the human retina (Figure S3).

MFAP4 binds endothelial integrin $\alpha_V\beta_3$ leading to FAK and ERK phosphorylation

The cellular distribution of MFAP4 expression in pericytes, SMCs, astrocytes, and Müller cells may allow locally secreted extracellular MFAP4 to interact with endothelial cells through integrin ligation and activation. We used primary human pulmonary microvascular endothelial cells (HPMECs) for our initial investigations of MFAP4s interaction with endothelial integrins. We showed that the microvascular endothelial cells adhered dose dependently to immobilized MFAP4 (Figure 2A) and that the adhesion was significantly inhibited by an integrin-antagonizing RGD peptide (Figure 2B). Integrin $\alpha_V\beta_3$ bound recombinant MFAP4 with the highest affinity among MFAP4-binding integrins also including $\alpha_V\beta_5$, $\alpha_V\beta_6$, and $\alpha IIb\beta_3$ (Figure 2C). No binding to other RGD-binding integrins was observed (Figure 2D). Focal adhesion kinase (FAK) and extracellular signal-regulated kinase (ERK) are known mediators of integrin signaling and their activation was increased by seeding microvascular endothelial cells on an MFAP4 matrix supporting that MFAP4's integrin binding led to integrin activation (Figures 2E and 2F).

The AS0326 antibody blocks MFAP4s interaction with endothelial integrins

Immunization of MFAP4-deficient mice with His-tagged recombinant human MFAP4 has been described previously.[15] We set out to analyze our panel of monoclonal anti-MFAP4 antibody-producing hybridoma cells to identify an MFAP4-blocking antibody. The monoclonal mouse antibody mAS0326 was selected among 17 hybridomas due to high stability (stability to variation of pH and temperature and to shear stress) and the ability to block cellular binding to an MFAP4 matrix. MFAP4 matrix induces short-term cellular adhesion, important for focal adhesion formation involved in cellular proliferation and migration.[10] Such effect is common for a subset of ECM glycoproteins, also including vitronectin or fibronectin.[16] Initially, we demonstrated that both treatment with integrin $\alpha_V\beta_3$ or $\alpha_V\beta_5$-blocking antibodies (Figure 3A) as well as mAS0326 (Figure 3B) significantly reduced HPMEC adhesion to MFAP4. Importantly, integrins $\alpha_V\beta_3$ and $\alpha_V\beta_5$ were detected with comparable intensity in the endothelial cell culture (Figures 3C and 3D).

Before commencing humanization of mAS0326 to hAS0326 by complementarity-determining region (CDR) grafting, we showed that injection of a high dose of mAS0326 in rat eyes did not significantly affect hyperemia, chemosis, ERG profiles, or retinal morphology (Figure S4). There was no score >0 for discharge in any animal.

Endothelial cell proliferation and migration are essential functions contributing to choroidal neovascularization (CNV), which is a characteristic of nAMD. The neovascular vessels are leaky, causing exudation or retinal hemorrhage resulting in loss of vision.[17] Following, we investigated the effect of hAS0326 on VEGF-induced proliferation and migration of primary human microvascular retinal endothelial cells (RECs) seeded on an MFAP4 matrix or migrating toward an MFAP4 matrix *in vitro*, respectively. While hAS0326 tendentially reduced MFAP4-dependent REC proliferation in our analyses (Figure 3E), MFAP4-dependent migration was significantly inhibited by hAS0326 (Figures 3F–3H).

Specificity of the AS0326 antibody

Both mAS0326 and hAS0326 reacted with wild-type (WT) mouse serum but not with MFAP4-deficient mouse serum (Figures 4A and 4B). The half maximal inhibitory concentration (IC50) to inhibit binding of 1.5 nM MFAP4 to an excess of immobilized integrin $\alpha_V\beta_3$ was 8.8 nM for hAS0326 fragment antigen-binding (Fab) domain. No inhibition was observed when applying hAS0326Y94 A L-CDR3 negative-control Fab variant (Figure 4C).

Blocking of RGD-dependent integrins is typically mediated through neutralization of the RGD-binding site. However, mAS0326 and hAS0326 binding to MFAP4 was independent of the presence of RGD sequence in MFAP4, whereas control anti-MFAP4 antibody HG-HYB7-5 binding was dependent on the presence of RGD sequence (Figure 4D). m/hAS0326 was selected over HG-HYB7-5 because m/hAS0326 reacted with mouse MFAP4 and because the binding to immobilized human MFAP4 was stronger relative to HG-HYB7-5 (Figures 4E and 4F).

Epitope mapping demonstrated unique specificity of mAS0326 and hAS0326 relative to control anti-MFAP4 antibodies HG-HYB7-5 and HG-HYB7-18 (Figures S5A–S5C). As expected, the immunohistochemical reactivity of hAS0326 was similar to the previously published HG-HYB7-14 anti-MFAP4 antibody-binding profile with intense detection of MFAP4 in the ECM of elastic alveolar septa and arteries/arterioles[12] (Figures S5D–S5K). No detection was

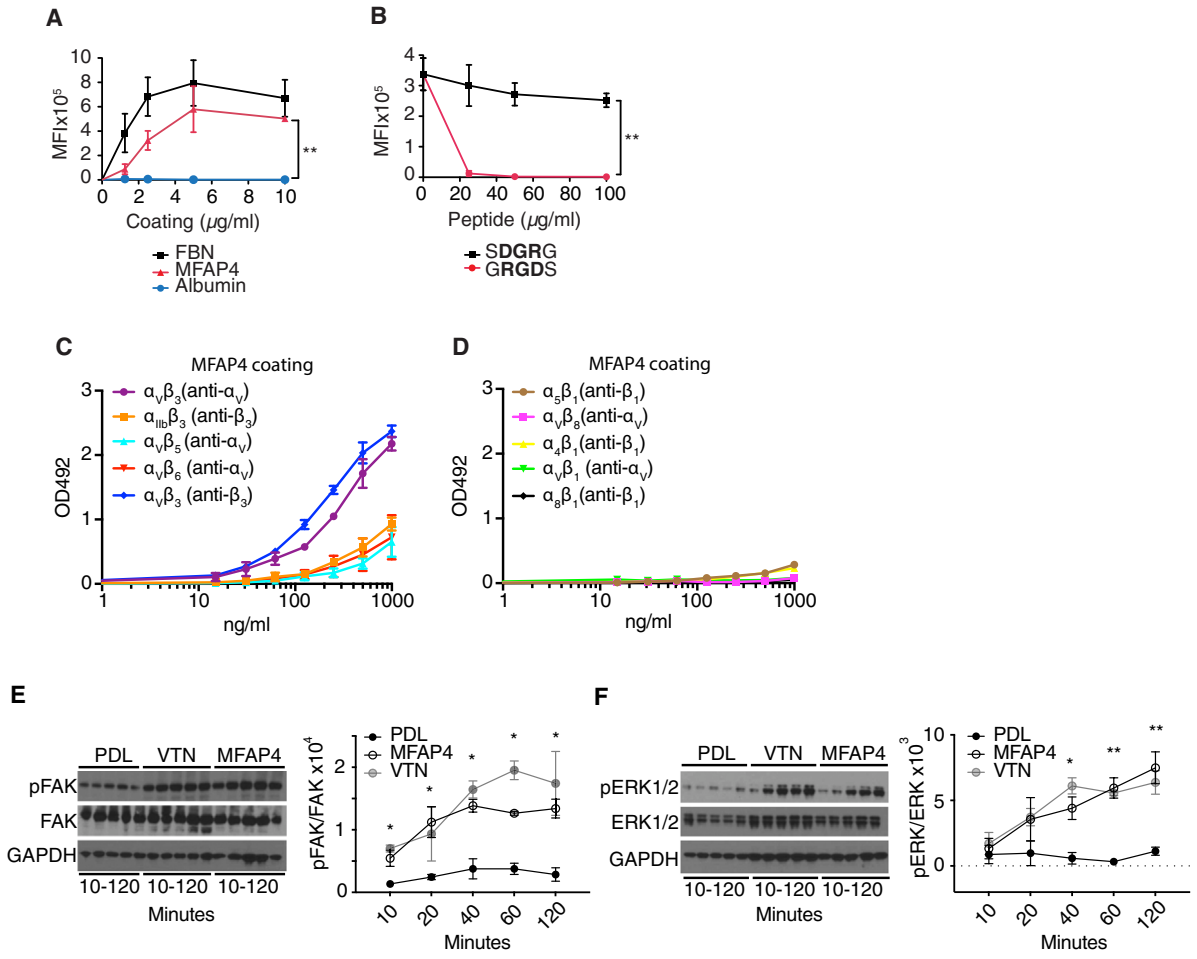

Figure 2. MFAP4 binding and activation of RGD-dependent integrins

(A) MFAP4 promotes adhesion of human pulmonary microvascular endothelial cells (HPMECs) in a dose-dependent manner. (B) MFAP4-mediated adhesion of HPMEC can be inhibited by RGD-containing peptide (GRGDS) but not control (SDGRG) peptide. Data are means (SD) of $n = 3$ independent experiments. Significance is calculated by two-way ANOVA. MFI, mean fluorescence intensity. Immobilized recombinant MFAP4 (2 μg/mL) was incubated with increasing concentrations of recombinant integrins. Integrin binding to recombinant MFAP4 was detected for (C) integrins $\alpha_V\beta_{3/5/6}$ and $\alpha IIb\beta_3$ but not (D) integrins $\alpha_V\beta_{1/8}$ and $\alpha_{4/5/8}\beta_1$. Used detection antibodies are shown in brackets. Data are shown as means (SD) of $n = 3$ independent experiments. Relative band density of (E) phosphorylated FAK (pFAK)/total FAK and (F) pERK/total ERK in HPMEC after cellular adhesion to poly-D-lysine (PDL, negative control), vitronectin (VTN, positive control), or MFAP4 are shown in representative western blots and quantitated mean (SD) of $n = 3$ independent experiments. Quantifications of western blotting was analyzed by two-way ANOVA for MFAP4 relative to negative control and the significance is provided for treatment factor only (independent of the significant time factor).

observed in MFAP4-deficient tissues (Figures S5E and S5I). These observations supported MFAP4 specificity of hAS0326.

Structure of the hAS0326 fragment antigen-binding-MFAP4 complex

We applied X-ray crystallography to characterize the binding interaction between MFAP4 and hAS0326. Crystallography data collection and refinement statistics are shown in Table S2. Crystals of the hAS0326 Fab-MFAP4 complex diffracted X-rays to a resolution of 3.4 Å. We identified eight copies of the Fab-MFAP4 complexes in the asymmetric unit of the crystal with only minor deviations between these eight complexes (Figures 5A–5E). Each Fab is in contact with a single MFAP4 subunit (Figures 5A, 5B, and 5E). The MFAP4 Ca^{2+} site is located opposite to the Fab paratope (Figure 5B). The fold of MFAP4 is, as expected from the high sequence homology, very similar to that of another protein from the fibrinogen-related domain superfamily, fibrinogen C domain-containing 1 (FIBCD1)[18] (Figures S6A and S6B). Each MFAP4 subunit binds a Ca^{2+} ion coordinated by main-chain oxygens from Phe174 and Gln176 and side chains from Asp170 and Asp172 (Figures S6C and S6D).

Eight MFAP4 molecules form a sphere-shaped hollow octamer with an outer radius of 50 Å and an internal cavity with a radius of 12 Å

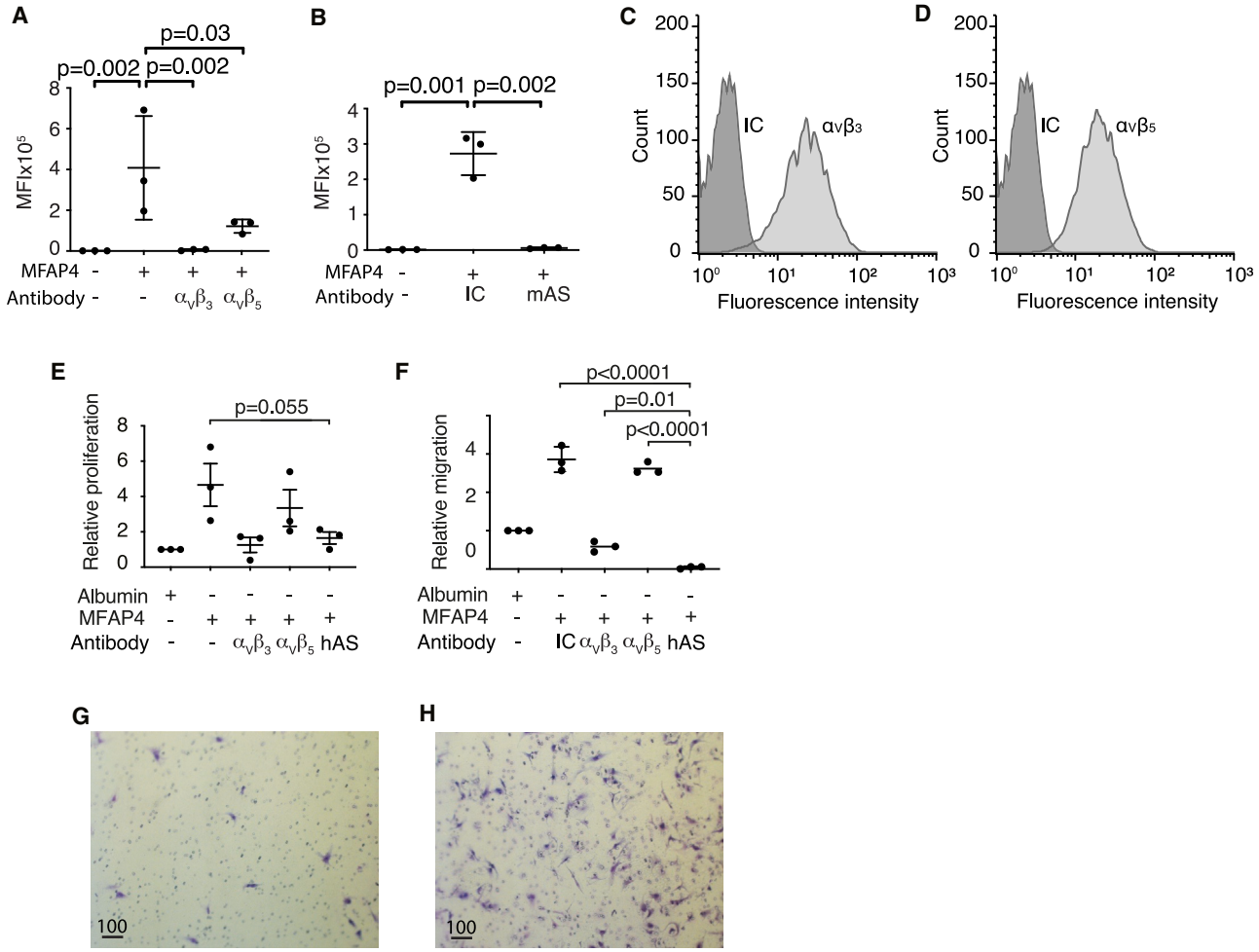

Figure 3. The AS0326 antibody blocks MFAP4s interaction with endothelial integrins

(A) HPMECs were subjected to MFAP4-mediated adhesion, and inhibition of adhesion was tested with integrin $\alpha_V\beta_3$- or integrin $\alpha_V\beta_5$-blocking antibodies. (B) mAS0326 antibody (mAS) blocks HPMEC adhesion to MFAP4. MFI is of fluorescently labeled cells. IC, isotype control. Significance is calculated relative to the MFAP4-treated positive control in (A) and (B). Flow cytometry staining of (C) integrin $\alpha_V\beta_3$ and (D) integrin $\alpha_V\beta_5$ in HPMEC compared to IC. Representative histograms of $n = 3$ independent experiments are shown. Human primary retinal endothelial cells (RECs) were seeded on immobilized albumin or MFAP4. RECs were stimulated with VEGF and 24-h proliferation was assessed. (E) REC proliferation was co-treated with integrin $\alpha_V\beta_3$- or $\alpha_V\beta_5$-blocking antibodies or hAS0326 (hAS). REC migration for 3.5 h on MFAP4-coated surface was assessed by Transwell assay using VEGF as chemoattractant. (F) MFAP4-dependent migration was treated with integrin $\alpha_V\beta_3$- or $\alpha_V\beta_5$-blocking antibodies or hAS0326. Data are shown as individual datapoints with mean (SD) of $n = 3$ independent experiments. Data are normalized to albumin control. Significance is calculated relative to the hAS0326 treatment group for (E) and (F). Significance calculations are performed using one-way ANOVA followed by Dunnett's multiple comparison test. Representative images of REC's (purple) migrated through the pores of the Transwell assay inserts when migration on (G) albumin-coated insert or (H) MFAP4-coated insert. Bar, 100 μm. All antibodies were provided in 10 μg/mL doses for (A), (B), (E), and (F).

(Figures 5C and 5D). The octamer is formed from two ring-shaped tetramers that are related by a 2-fold symmetry. Each ring has a convex and concave surface, the latter forming one-half of the internal cavity (Figure 5D), whereas four copies of the N-terminal residues Leu14-Ser30 form the top of the convex surface. Based on the high structural similarity with FIBCD1, it is furthermore possible to suggest a putative binding site (S1) for ECM or carbohydrate ligands (Figure S6E) in a location close to the Ca^{2+}-binding site. In the MFAP4 octamer, two possible S1 sites at the tetramer-tetramer interface are separated by 21–23 Å.

Paratope and epitope description of the Fab-MFAP4 complex

In MFAP4, the 13–15 N-terminal residues including the integrin-binding RGD motif could not be modeled, suggesting they are flexible. In the Fab-bound MFAP4 octamer, they appear to be located inside a funnel formed by four Fab molecules, all binding on the same face of the tetramer (Figure 5E). This supports that steric hindrance contributes to the mechanism whereby hAS0326 impairs interaction between MFAP4 and the integrin receptor. The paratope contains residues from all three Fab heavy-chain (H)-CDRs while the light chain (L)-CDR1 and CDR3 form contacts with MFAP4. The epitope

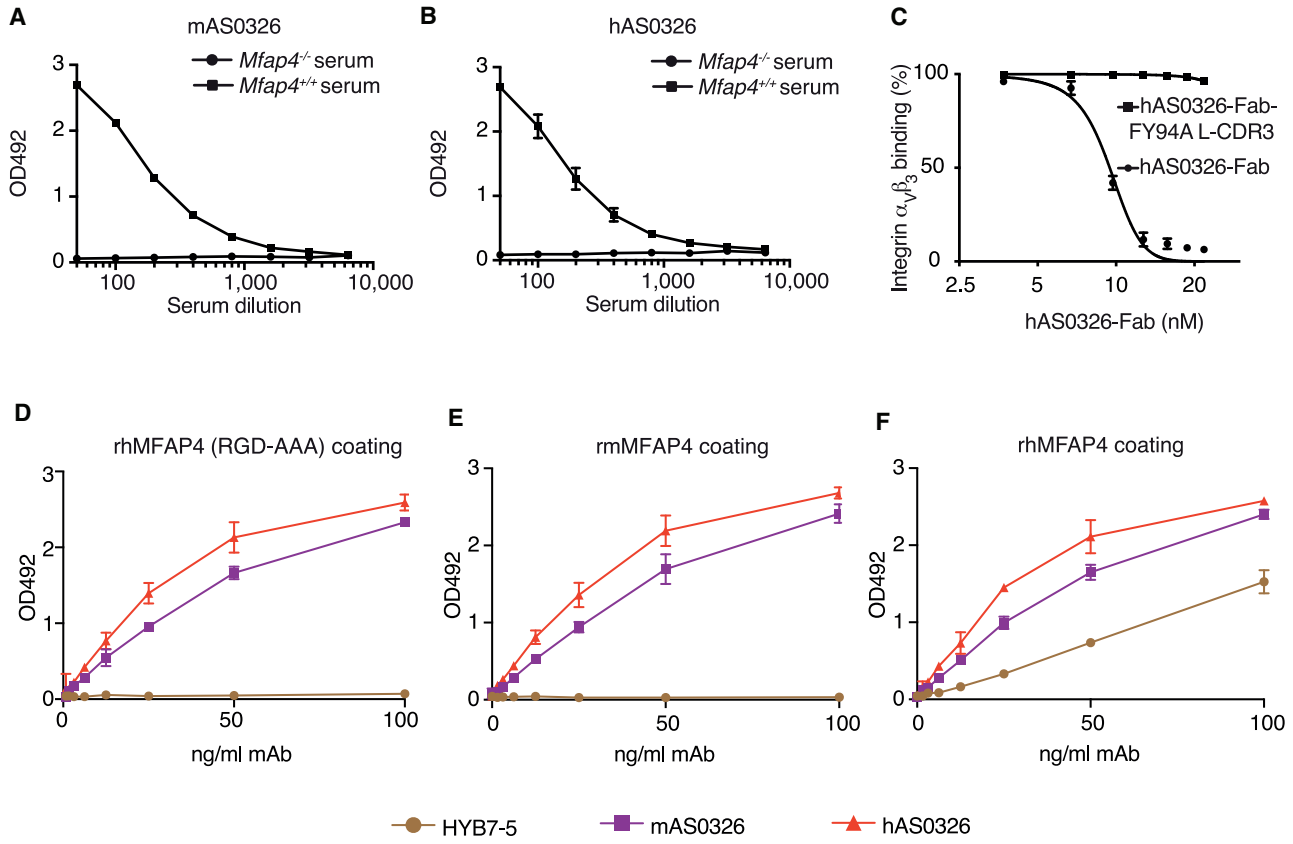

Figure 4. Specificity of the AS0326 antibody

(A) mAS0326 and (B) hAS0326 efficiently detect MFAP4 in WT (*Mfap4*$^{+/+}$) mouse serum, but not in MFAP4-deficient (*Mfap4*$^{-/-}$) mouse serum. (C) Increasing concentrations of hAS0326-Fab or hAS0326Y94A L-CDR3 Fab variant were applied for inhibition of 1.5 nM MFAP4 binding to an excess of immobilized integrin $\alpha_V\beta_3$. (D–F) Brown symbols, HG-HYB7-5; purple symbols, mAS0326; red symbols; hAS0326. (D) Both mAS0326 and hAS0326 efficiently detect immobilized recombinant human MFAP4 (rhMFAP4 coating) variant carrying RGD-AAA mutation (RGD-AAA), while HG-HYB7-5 antibody show RGD-dependent binding. Both mAS0326 and hAS0326 efficiently detect immobilized (E) recombinant mouse (rm) MFAP4, and (F) rhMFAP4, while HG-HYB7-5 is rhMFAP4 specific. Data are shown as means (SD) of $n = 3$ independent experiments.

encompasses primarily the MFAP4 residues Tyr24, Ala25, Gln26, Gly27, Tyr28, Gln29, Glu54, Gly55, Lys57, and the two C-terminal residues Arg233-Arg234 (Figure 5F). The interface area between MFAP4 and the Fab is ∼700 Å. The interaction is centered at the insertion of MFAP4 Tyr24 into a pocket formed by H-CDR3 Trp107 and H-CDR1 Trp33, and the phenolic alcohol of Tyr24 engages in hydrogen bonding with the side chain of H-CDR3 Glu99 (Figure 5G). The main chain of MFAP4 Tyr24 also appears to form a hydrogen bond with the side chain of H-CDR1 Trp33. Although not in direct contact with MFAP4, H-CDR3 Trp101 borders the binding pocket for the small α helix containing MFAP4 residues Asp21-Gln26. The neighboring H-CDR3 Tyr103 appears to form van der Waals interactions with the two C-terminal MFAP4 residues Arg233-Ala234. Side chains in H-CDR2 form hydrogen bonds with the main-chain carbonyls of MFAP4 Ala25, Gln26 and Gly27 (Figure 5G). In L-CDR3, Tyr94 stabilizes the position of H-CDR3 Trp107, which, in addition to the already-mentioned contacts with MFAP4 Tyr24, also engages with MFAP4 Gly55 through van der Waals interactions (Figure 5G).

Importantly for hAS0326 efficacy testing *in vivo*, the MFAP4 protein has high sequence homology with MFAP4 from other vertebrate species. When comparing the 13 amino acid residues, which are primarily in contact with heavy-chain and light-chain CDRs in hAS0326, the following sequence homologies were observed: mouse (100%), rat (91%), rabbit (100%), and green monkey (100%) (obtained from https://blast.ncbi.nlm.nih.gov/Blast.cgi). The AS0326 antibody was raised in *Mfap4*-deficient mice and therefore it also can show immunoreactivity toward mouse MFAP4.

Validation of the hAS0326 paratope

The dissociation constant (K_D) for the complex between MFAP4 and hAS0326 was $7.37 \cdot \times 10^{-11} \pm 0.91 \cdot 10^{-11}$ M versus $2.21 \cdot \times 10^{-10} \pm 0.14 \cdot 10^{-10}$ M for hAS0326 Fab, in accordance with a bivalent interaction of hAS0326 with MFAP4 (Table S3). Five paratope residues of the hAS0326-MFAP4 interface were point mutated and the resulting Fabs showed 5- to 300-fold increased K_D relative to hAS0326 Fab (Table S3). Representative sensorgrams are presented in Figure S7 together with fitted binding curves.

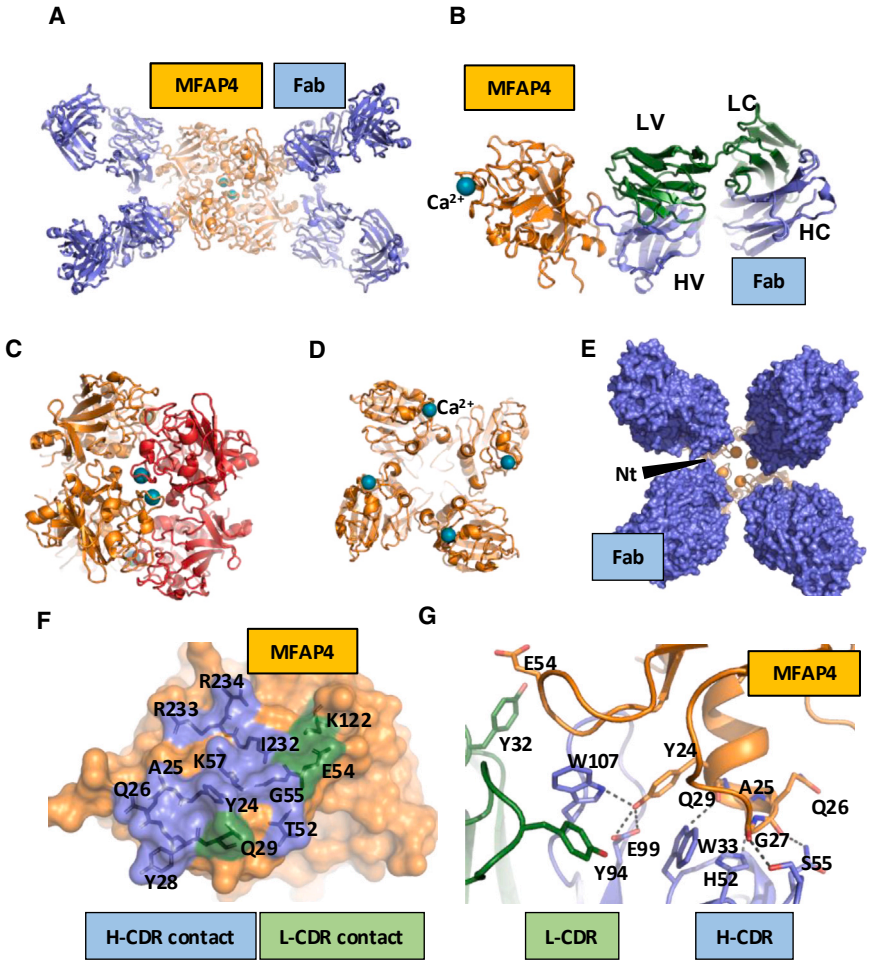

Figure 5. Structural basis for the hAS0326 Fab interaction with MFAP4

The hAS0326 Fab complex and the MFAP4 octamer. (A) Cartoon representation of the octameric MFAP4-Fab complex. (B) Each Fab contacts a single MFAP4 monomer at an epitope next to the MFAP4 N terminus but far from the binding site for the Ca^{2+} ion (cyan sphere). (C) The MFAP4 octamer is built from two FIBCD1-like tetramers (colored orange and red) with eight Ca^{2+} ions located at the tetramer-tetramer interface. (D) Inside view showing the concave face of the tetramer. (E) Top view of the convex face of the tetramer with the four bound Fab molecules. Orange spheres mark the first MFAP4 residue that can be located. Presumably, the disordered RGD integrin-binding motif at the N terminus of MFAP4 is trapped and inaccessible inside the funnel-shaped space formed by the Fab molecules. Nt, N terminus. (F) The epitope mapped on MFAP4. Residues primarily in contact with heavy-chain and light-chain CDRs are colored blue and green, respectively. (G) Details of the intermolecular interaction centered on MFAP4 residues 24–29. Putative polar interactions are indicated by dotted lines.

hAS0326 reduces mouse laser-induced CNV lesion size

Following, we analyzed the efficacy of hAS0326 in limiting neovascularization in a mouse model of laser-induced CNV (Figure 6A). Representative images of fundus fluorescein angiography (FFA)-defined lesion area and isolectin B4 (IB4) stainings are shown in Figures 6B and 6C. The efficacy of i.v.t. hAS0326 in limiting the vascular lesion area was measured by FFA-defined lesion area 14 days after laser-induced CNV in mice (Figure 6D). Similar data were observed 7 days after laser-induced CNV (Figure S8). Positive control for reduction of FFA was treatment with a neutralizing, experimental anti-VEGF antibody. Treatment with 1 μg or 5 μg hAS0326 significantly reduced the FFA lesion area relative to the negative control (vehicle) treatment (Figure 6D). Also, treatment with 1 μg or 5 μg hAS0326 significantly reduced the isolectin B4 (IB4)-positive neovessel volume (Figure 6E) relative to the negative control.

i.v.t. hAS0326 reduces vascular permeability in a rat model of hyperglycemia-induced retinopathy

The role of integrin $\alpha_V\beta_3$ in vascular leakage has provided contradictory observations.[19–21] However, inhibition of integrins $\alpha_V\beta_3$ and $\alpha_V\beta_5$ is considered beneficial in DME.[5] On this basis, we tested the effect of blocking MFAP4-integrin ligation in a model of hyperglycemia-induced retinopathy. Rats were injected with streptozotocin (STZ; 50 mg/kg), causing insulin deficiency. On day 4 after STZ injection, average plasma glucose levels were 25.6 ± 2.5 mg/dL, while age-matched control rats had glucose levels within normal limits (8.4 ± 1.2 mg/dL). These levels were maintained throughout the duration of the study. The animals were maintained for 21 days with subcutaneous insulin supplementation and diabetic and non-diabetic rats weighed 312.8 ± 3.0 g and 277.9 ± 4.4 g, respectively. Day 0 and day 7 after STZ injection, animals received i.v.t. saline, anti-VEGF (1 μg), or hAS0326 (1 μg or 5 μg) (Figure 6F). The vascular permeability was following monitored in a time series (Figure 6G). All treatments significantly reduced the day 21 FFA vascular permeability coefficient relative to the negative control (Figure 6H).

Tolerability and distribution of i.v.t. hAS0326

Tolerability of hAS0326 was tested at three doses (0.5 mg, 1.25 mg ,or 2 mg per 50 μL) after a single i.v.t. injection in the non-human primate (NHP) species the African green monkeys. The animals that received hAS0326 exhibited a similar level of mild intraocular inflammation peaking around day 2 compared to vehicle-injected animals. This consisted primarily of aqueous cells, with significant resolution by day 7 (Figure S9A). Intraocular pressure (IOP) (Figure S9B) and central retinal thickness (Figure S9C) remained stable over the course of the study. Representative images of fundus photography and optical coherence tomography are shown in Figures S9D and S9E. No evidence of systemic side effects was observed. Furthermore, we checked

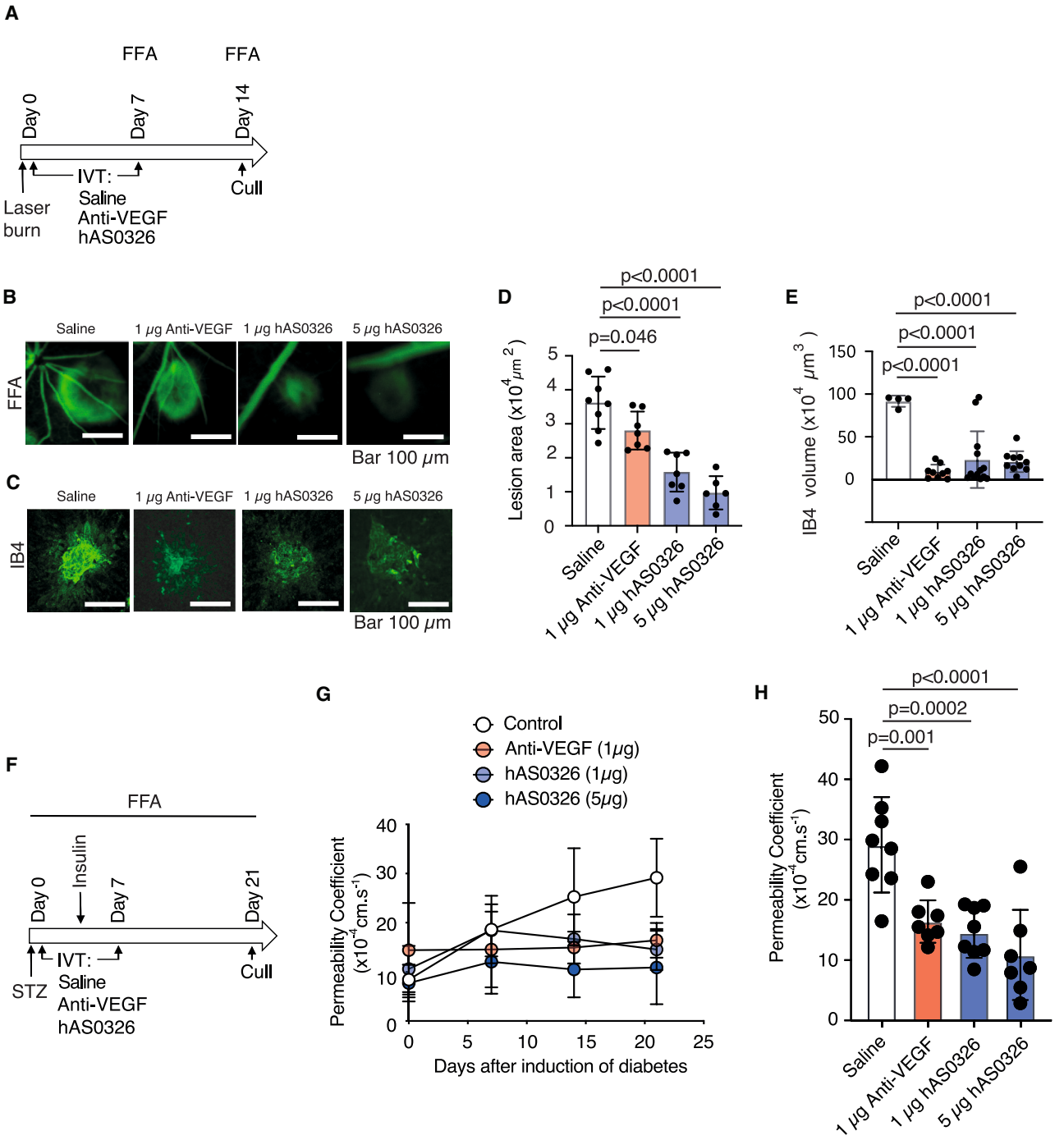

Figure 6. hAS0326 inhibits retinal vascular leakage in laser-induced mouse CNV and STZ-induced rat retinopathy

(A) i.v.t. hAS0326 injection was performed on day 0 and 7 after laser burn in a 14-day mouse laser-induced CNV model. Representative (B) FFA and (C) IB4-stained images on laser-induced lesions from the different treatment groups. (D) Quantification of lesion size by FFA or (E) vascular volume (IB4-positive volume). Each data point represents a mean of 1–4 lesions per eye, $n = 4–13$ animals/group. (F) Type 1 diabetes was induced in Norway brown rats following a dose of STZ (50 mg/kg) and animals were maintained for 21 days. i.v.t. hAS0326 injection was performed on day 0 and 7. (G) FFA was used to calculate the vascular permeability coefficient in a 21-day time course after induction of diabetes. (H) The vascular permeability coefficient day 21. $n = 7–8$ animals/group (one eye per animal). Individual data points are shown with mean (SD) for all animal experiments. Significance is calculated relative to saline treatment. Significance calculations are performed using one-way ANOVA followed by Dunnett's multiple comparison test.

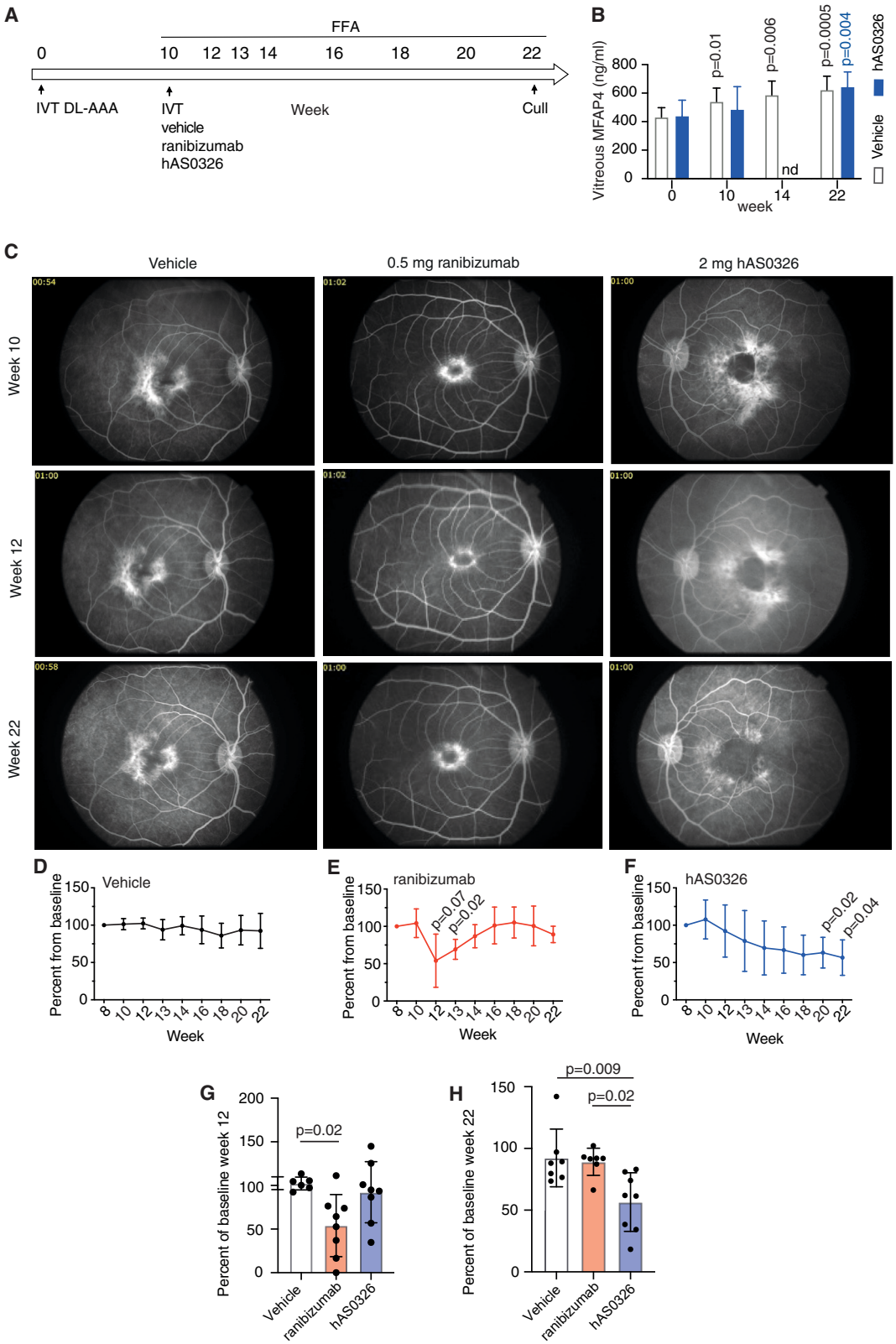

(legend on next page)

if i.v.t. hAS0326 could penetrate all treatment-relevant ocular layers of the rabbit eye, which has an ocular volume resembling that of the African green monkey. One week after i.v.t. injection of 2 mg of hAS0326, the rabbit eye showed intense and specific deposition of hAS0326 throughout the retina and the choroid (Figure S10).

i.v.t. hAS0326 reduces vascular leakage in an NHP model of chronic retinopathy

Finally, we applied the DL-2-aminoadipic acid (DL-AAA)-induced chronic retinopathy model in African green monkeys.[22] The advantages of the DL-AAA NHP model include genetic homology between primates and humans and the presence of a macula. Importantly, the DL-AAA model has the ability to characterize therapeutic effects during the late, stable stage of chronic disease and to test duration of efficacy of a single dose of therapy.

Characterization and stratification of enrolled animals are shown in Table S4. Stable hyperfluorescent leakage was predominant in the macular region 10 weeks after DL-AAA administration. By week 10, one i.v.t. injection of negative control (vehicle), positive control (0.5 mg ranibizumab), or 2 mg of hAS0326 (highest dose tested for tolerability) was administered. Retinal vascular leakage area was following monitored until week 22 (Figure 7A). Vitreous was tapped at week 0, 10, 14, and 22 and showed that the DL-AAA model induced a mild induction of MFAP4 from week 10 to week 22 in the vehicle-treated group, which was not detectable by week 14 in the hAS0326-treated group but returned by week 22 (Figure 7B).

Representative FFA images obtained by week 10, 12, and 22 are shown in Figure 7C. The relative leakage area did not change significantly from pre-dose level (week 10) throughout the study period in the vehicle group (Figure 7D). The leakage area was significantly reduced relative to pre-dose level by week 13 in the ranibizumab positive-control group even if higher mean reduction was observed at week 12 (Figure 7E). A linear decrease of relative vascular leakage area was observed in the hAS0326 treatment group between week 10 and week 14 and reached significantly reduced levels through weeks 20 and 22 relative to pre-dose level (Figure 7F). By week 12, ranibizumab treatment, but not hAS0326 treatment, produced significantly reduced leakage area compared with vehicle treatment (Figure 7G). Treatment effects of ranibizumab by week 12 were no longer significant ($p = 0.087$) when performing multiple linear regression and including treatment group, sex, weight, and age as covariates. Age was the only significant co-variant in that regression ($p = 0.047$). By week 22, the hAS0326 treatment produced significantly reduced leakage area compared with vehicle and ranibizumab treatment (Figure 7H). Treatment effect of hAS0326 by week 22 remained significant ($p = 0.0088$) when performing multiple linear regression and including treatment group, sex, weight, and age as covariates. No other covariate was significant in that regression.

The macular proteome of the DL-AAA-induced model of chronic retinopathy supports hAS0326-mediated integrin inhibition

Proteome analysis was performed on macular tissue punches (including choroid, retinal pigment epithelia [RPE], and retina) obtained at end-study of the above experiment. This analysis showed significant regulation of multiple molecular function Gene Ontology (GO) terms (Figure 8A).

Significantly upregulated molecular functions in DL-AAA treated eyes included cell adhesion molecule binding and integrin binding (Figure 8A). In contrast, these terms were significantly downregulated molecular functions by hAS0326, indicative of hAS0326-mediated reversal of such effects. Volcano plots highlighting proteins underlying these DL-AAA-enriched GO terms are shown in Figures 8B and 8C and the hAS0326-enriched GO terms in Figures 8D–8F. Proteins that were downregulated by hAS0326 included protein tyrosine phosphatase receptor type F (PTPRF) and interferon-stimulated gene 15 (ISG15) (Figures 8D and 8E).

The full list of identified proteins and their regulation for each treatment is provided in Table S5A, significantly regulated molecular function terms are provided in Table S5B, and most significantly regulated GO terms of additional categories are provided in Table S5C.

We specifically looked for regulation of MFAP4 and integrin $\alpha_V\beta_3$ in the proteomes, but these proteins were not detected by this method. Therefore, western blotting for MFAP4 and integrins was performed (Figures S11A and S11B). This analysis showed that MFAP4 was expressed with high variation between individual eyes in the vehicle-treated group relative to control eyes and ranibizumab- and hAS0326-treated eyes in the week 22 samples (Figure S11C). Integrin β_3 was not regulated in the week 22 samples, but integrins α_V and β_5

Figure 7. i.v.t. hAS0326 reduces DL-AAA-induced retinal vascular leakage area in non-human primates

(A) i.v.t. DL-AAA was provided in week 0 in each eye of African green monkeys. Eyes were randomized into treatment groups and 50 μL of vehicle, ranibizumab (positive control, 0.5 mg), or hAS0326 (2 mg) was administered i.v.t. by week 10. FFA imaging was obtained at week 8 post DL-AAA administration (pre-dose) and eight times following i.v.t. treatments (weeks 10, 12, 13, 14, 16, 18, 20, and 22). Fluorescein leakage was assessed by computer-based analysis of 1-min FFA intensity. (B) Vitreous MFAP4 levels are shown as means (SD) from week 0–22. Significance is calculated for the difference in MFAP4 levels at individual time points relative to week 0 in the two treatment groups. Significance was calculated by mixed-effects analysis followed by Dunnett's multiple comparison test. Nd, not detected. (C) Representative FFA images obtained in week 10 (pre-dose), week 12 (maximal positive control efficacy), and week 22 (end of study) are shown for each treatment group. (D–F) Relative FFA-defined leakage areas in percentage of pre-dose area are shown as means (SD) from week 10–22 for vehicle, ranibizumab, and hAS0326 treatment, respectively. Data are normalized to the pre-dose leakage area. Significance is calculated for the difference in leakage from individual time points relative to week 10 in the respective treatment groups. Significance is estimated by mixed-effects analysis followed by Dunnett's multiple comparison test. Relative leakage areas in percentage of pre-dose area (G) week 12 or (H) week 22. Individual data points are shown with mean (SD). Significance calculations are performed using one-way ANOVA followed by Tukey's multiple comparison test. $n = 6–8$ eyes/group.

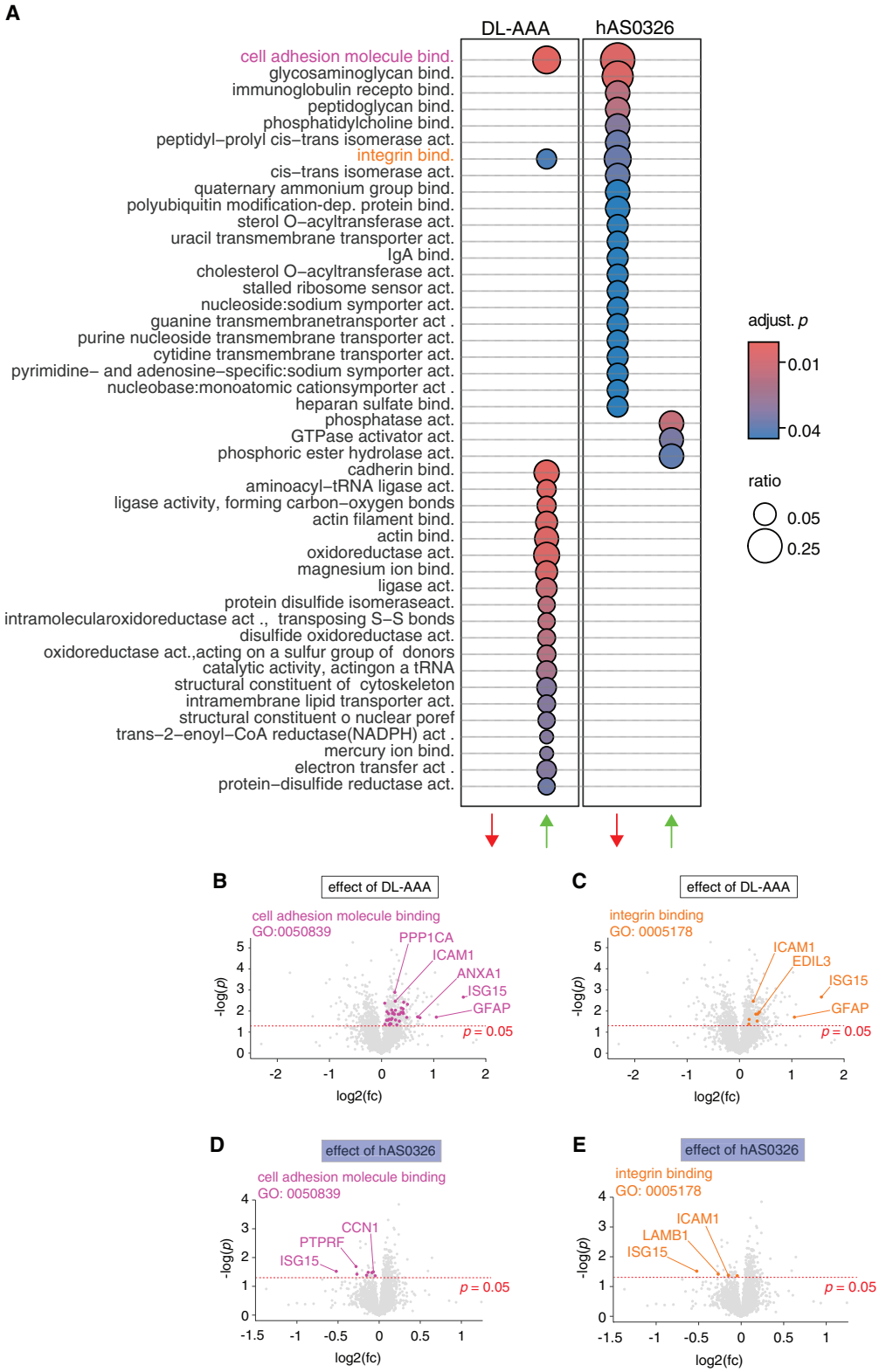

(legend on next page)

were significantly induced by ranibizumab- relative to control-treated eyes (Figures S11D–S11F).

Pharmacokinetics of hAS0326 in NHP

We analyzed the elimination of hAS0326 from ocular tissue to further characterize this antibody and to explore a potential cause of the observed long duration of efficacy of at least 12 weeks. A mean of 383 μg/mL free hAS0326 was retrieved in the vitreous humor on day 1 after a single i.v.t. injection of 2 mg (Figure S12A). Half-life of free hAS0326 was 3.88 days (95% confidence interval [CI] [3.01:5.01] days) when calculated as one-phase decay in the vitreous humor. The initial half-life of hAS0326 in the combined retinal, RPE, and choroid tissue lysate (ocular tissue lysate) was 3.19 days (95% CI [2.37:4.32] days) when calculated by a two-phase decay model (Figure S12B). The second phase of decay was not possible to estimate as only two measurement points (day 35 and day 63) were available. However, approximately 5 ng/mg of hAS0326 remained in the ocular tissue lysate day 35–63 after a single injection.

DISCUSSION

In this study, we found that the extracellular matrix glycoprotein MFAP4 is expressed in endothelial neighboring cells in the choroid and the retina in control, DR, and AMD eyes. We developed a humanized monoclonal anti-MFAP4 antibody, hAS0326, blocking MFAP4's interaction with RGD-dependent integrins including $\alpha_V\beta_3$ and $\alpha_V\beta_5$. This antibody reduced MFAP4-dependent endothelial motility *in vitro* with mechanistic relevance for neovascularization and vascular leakage. i.v.t. delivery of hAS0326 reduced CNV and retinal vascular leakage in independent animal models and was tested in three different species. A single hAS0326 i.v.t. injection showed duration of efficacy of 3 months in reducing chronic retinal vascular leakage in NHP. Taken together, MFAP4 has potential as target and hAS0326 shows potential as i.v.t. therapy for reduction of retinal neovascularization and retinal vascular leakage.

Pericytes, SMCs, Müller cells, and astrocytes showed *MFAP4* expression. Recent findings support that pericytes,[23] astrocytes,[24] and Müller cells[25] play key roles in retinal disease development characterized by neovascularization and vascular leakage. Importantly, all these cell types may deposit MFAP4 in close proximity to endothelial cells with relevance for development of neovascularization and vascular leakage. Also, fibroblasts were observed as major contributors to MFAP4 expression. A role of MFAP4 as aggravator of fibrosis was recently demonstrated,[26,27] but investigation of this potential role was out of the scope of the present study.

Moreover, we have previously demonstrated that MFAP4 enhances monocytic migration.[10] Future studies on the potential role of MFAP4 as aggravator of retinal or choroidal inflammation could therefore involve investigations of MFAP4-dependent recruitment of monocytes into CNV lesions. Investigation of MFAP4's potential activation of Müller cell- or astrocyte-mediated inflammation would also be relevant for future studies of retinal inflammation due to the observed MFAP4 expression in these cell types.

We did not observe changes in vitreous levels of MFAP4 between clinical retinal diseases. Additionally, we previously observed that MFAP4 did not differ significantly between nAMD and controls in human vitreous collected during elective cataract surgery and pars plana vitrectomy.[28] Our present *in situ* hybridization analysis of MFAP4 expression in human eyes neither excluded nor revealed changes in MFAP4 expression in the ocular tissue between control and disease. This may suggest that retinal MFAP4-regulation is limited in retinal disease and that involvement in retinal disease depends on the expression of cellular RGD-dependent integrins, which are known to be induced by the disease.[29] Meanwhile, the basal level of ocular MFAP4 expression may allow long-term target-mediated drug deposition of antibodies binding MFAP4 in the retinal and choroidal ECM and with potential relevance for the observed long duration of efficacy of hAS0326. In this regard, low levels of hAS0326 were retained in the macular tissue 3 months after single i.v.t. administration in NHP eyes.

Our X-ray crystallographic study revealed that hAS0326 makes MFAP4 inaccessible for integrin receptor interaction through steric hindrance. Recently, a highly similar cryoelectron microscopy-derived structure of MFAP4 was published.[30] The previous study demonstrated that MFAP4's cellular interaction was reduced by fibrillin, which binds MFAP4 in close proximity to the RGD sequence. It was also shown that MFAP4 has multiple interfaces for interacting with ECM fibrils and the interaction with integrins in the presence of other type of fibril binding was not explored. We demonstrated that hAS0326 is capable of binding MFAP4 deposited in the ECM and thereby blocking MFAP4 present in the ECM.

We observed that integrin $\alpha_V\beta_3$ inhibition attenuates the MFAP4-related endothelial cell responses *in vitro*. An effect of integrin $\alpha_V\beta_5$

Figure 8. The macular proteome of the DL-AAA-induced model of chronic retinopathy supports integrin involvement

Macular punches including choroid, RPE, and retina obtained at end-study (week 22) were analyzed by mass spectrometry and following analysis using clusterProfiler 4.0 package in R. The proteomes were generated from $n = 3$ eyes for non-diseased control, $n = 5$ eyes for DL-AAA treatment, and $n = 5$ eyes for hAS0326 treatment. (A) Over-representation analysis (ORA) showing the effect of DL-AAA treatment (relative to no DL-AAA treatment) and hAS0326 treatment of DL-AAA-treated eyes (relative to DL-AAA treatment), respectively. The plot was generated using compareCluster function with default settings. All ontologies with significant regulation post correction for multiple testing using the Benjamini-Hochberg procedure are shown. Dot sizes indicate the ratio (i.e., the coverage of a given term by proteins regulated for each comparison), and dot colors indicate the level of significance. (B–E) Volcano plots showing regulation of detected proteins underlying selected GO terms. For selected, significantly regulated gene ontologies, the ORA input proteins displaying significant regulation are highlighted in color. Protein IDs are shown for the top three proteins with lowest p belonging to a particular ontology. Moreover, protein IDs are shown for specific proteins of interest.

blocking was also observed but was less efficient in the performed cell cultures. VEGF-driven endothelial cell activation together with *de novo* expression of integrin $\alpha_V\beta_3$ is a principal underlying cause of neovascularization and vascular permeability, and VEGF-signaling is further dependent on integrin $\alpha_V\beta_5$.[31] In the present study, we demonstrated that endothelial cells bind to MFAP4 through RGD-dependent integrins leading to activation of cellular signaling implicated in neovascularization and vascular leakage.[32] In line with this, laser-induced CNV, STZ-induced retinopathy, and DL-AAA-induced retinopathy models supported a pathological role of MFAP4 in retinal neovascularization and vascular leakage and showed significant therapeutic effects of hAS0326.

While the applied rodent models of retinopathy are of relatively short duration (few weeks), the DL-AAA model of retinopathy is characterized by pathological vascular remodeling with persistent retinal neovascularization and vascular leakage[22] and was initially developed to study long-acting anti-VEGF therapies.[33] The utilized DL-AAA model produced a slight increase in MFAP4 vitreous levels throughout the 22-week-long model indicative of a relatively high basal level and an additionally model-induced synthesis. We applied this model in order to test therapeutic efficacy in NHP and duration of hAS0326 efficacy in chronic retinopathy. The kinetics of the treatment responses were different between hAS0326 and the positive-control ranibizumab. An initial linear decrease of the vascular leakage area was observed in the 2 mg hAS0326 (highest tested dose in tolerability study) treatment group 1–4 weeks after i.v.t. injection and a sustained reduction of the vascular leakage area was reached 8–12 weeks after i.v.t. injection. The positive control 0.5 mg (clinical dose) ranibizumab showed maximal efficacy 2–3 weeks after i.v.t. injection, which following leveled off. In comparison, 1.4 mg of aflibercept has previously shown maximal (approximately 50%) reduction of fundus fluorescence intensity 2–4 weeks after i.v.t. injection in the NHP DL-AAA model.[22] We conclude that i.v.t. hAS0326 intervention reduces the vascular leakage in the macular area with a slow onset and for at least 12 weeks after injection. We speculate that the slow onset potentially reflects that integrin-bound MFAP4 only gradually becomes available for blockade by hAS0326.

Enriched GO terms and significant proteins regulated by disease and hAS0326 were investigated at end-study in the DL-AAA model. "Cell adhesion molecule binding" and "integrin binding" were among the top upregulated molecular function GO terms by DL-AAA-induced disease (vehicle-treated group). These and additional disease-enriched terms comprised significant upregulation of proteins involved in cytoskeletal changes, proteosome activity, membrane lipid asymmetry, photoreceptor function, antioxidant/redox regulation, protein synthesis, inflammation, and gliosis. These effects are likely contributing to the overall sustained pathology of DL-AAA and warrant further characterization. However, we specifically used proteome analysis to study disease-induced effects that were reversed by hAS0326. hAS0326 intervention showed significant downregulation of GO terms "cell adhesion molecule binding" and "integrin binding." Most significantly downregulated proteins included PTPRF and ISG15, which are involved in integrin-dependent focal adhesion formation, cell adhesion, and migration.[34,35] Thus, hAS0326-regulated GO terms are likely reflecting aspects of disease-induced altered cell motility and vascular leakage in support of observations obtained from our *in vitro* and *in vivo* models.

We analyzed MFAP4 and integrin expression in the NHP macular tissue using semi-quantitative western blotting. This analysis showed that MFAP4 showed a far higher variability in the vehicle-treated diseased group, relative to the control group and intervention groups, and suggested that MFAP4 was upregulated by the model by week 22, although to a variable degree. Integrin β_3 was not regulated at this time point, while integrin α_V and β_5 were induced by ranibizumab and maybe this observation partly explains the loss of ranibizumab efficacy by week 22 in the DL-AAA model.

A model of MFAP4- and hAS0326-mediated effects in DL-AAA-induced retinal disease is shown in Figure S13.

In our NHP tolerability study, we observed transient, mild inflammatory cell infiltration day 2 after i.v.t. injection of hAS0326. The observation is in line with observations performed during preclinical development of anti-VEGF therapy for retinal disease.[36] Further development of hAS0326 may include introducing specific mutations, which prevents the binding to Fcγ receptors, such as mutations introduced in the retinal therapy faricimab to reduce the possibility of an undesirable immune system response.[37]

Four weeks after i.v.t. injection of hAS0326 (week 14), there was no immunodetection of vitreous MFAP4 in the DL-AAA model. However, vitreous MFAP4 levels were retrieved again by the end of the study (week 22). These data suggest that ocular MFAP4 epitopes were saturated with hAS036 by week 14 but no longer by week 22. The observation warrants testing of higher or sequential dosing of hAS0326 in future intervention studies. Moreover, future studies comparing the effect of hAS0326 in retinal disease models against VEGF-neutralizing therapies aflibercept or faricimab or integrin inhibitors are also warranted.

While measurement of MFAP4 in vitreous may not be relevant in a clinical setting, we recently observed that MFAP4 was also detectable in aqueous fluid.[28] Thus, aqueous fluid MFAP4 measurements may potentially serve as marker for human ocular saturation with hAS0326.

RGD-dependent integrins have various different ECM-ligands[38] and it is not fully clear how an individual integrin can discriminate between different ligands. One explanation has come from a recent study demonstrating that varying the mechanical load on integrin $\alpha_V\beta_3$ enabled differential ligand specificity.[39] We observed that blocking MFAP4 alone was effective in reduction of neovascularization and vascular leakage in the applied animal models. In line with this, we have previously used a model of human saphenous vein organ culture *ex vivo* and showed that therapeutic blocking of MFAP4 resulted in

almost complete inhibition of neointimal growth in this clinically relevant tissue.[10] Our combined observations suggest MFAP4 to be essential for these investigated pathological vascular processes. Importantly, we cannot exclude that co-inhibition of additional vascular integrin ligands or cotreatment with direct integrin inhibitors could enhance hAS0326 therapeutic efficacy further.

While integrin $\alpha_V\beta_3$ ablation has shown increase of vascular permeability,[19] pharmacological inhibition of RGD-dependent integrins has uniformly shown reduction of neovascularization and vascular leakage.[29] Importantly, clinical trials have supported safety of integrin inhibition in the human eye.

Risuteganib (ALG-1001/Luminate, Allegro Ophthalmics), is an inhibitor of integrins $\alpha_V\beta_3$, $\alpha_V\beta_5$, $\alpha_5\beta_1$, and $\alpha_3\beta_1$.[40] Risuteganib has been examined in clinical phase 1/2 studies for nAMD and results demonstrated a mean best corrected visual acuity (BCVA) improvement of five letters, 30% decrease in central macular thickness (CMT), and no associated adverse events.[41] Moreover, risuteganib was examined in a randomized prospective phase 2 trial evaluating its safety and efficacy in DME patients. The primary endpoint of noninferiority in BCVA and CMT improvement compared to bevacizumab was met.[42]

Topical administration of nesvategrast (SF0166/OTT166, SciFluor Life Science and Ocuterra), an integrin $\alpha_V\beta_{3/6/8}$ antagonist, has been applied.[43] Ocuterra recently announced that nesvategrast failed to demonstrate a statistically significant improvement on the DR severity scale versus placebo despite positive safety and tolerability in DME and wet AMD patients.[44]

A limitation of the present study is that we did not test if *Mfap4* deficiency would affect retinal disease development. MFAP4 has independent functions in ECM organization[9] and integrin activation. We chose to focus on intervention with hAS0326 blocking the MFAP4's interaction with integrin alone and thereby to study the disease models without confounding effects from ECM disorganization due to *Mfap4* deficiency. A translational limitation is that we used experimental anti-VEGF in the rodent models. The rodent models therefore have capacity to demonstrate therapeutic efficacy of hAS0326, while comparison to the efficacy of anti-VEGF is not relevant. Another limitation is that we did not use human immunoglobulin (Ig)G control for the presented *in vivo* intervention studies.

In conclusion, hAS0326-mediated blocking of MFAP4 binding to RGD-dependent integrins results in long-lasting therapeutic effects. The deposition of hAS0326 by high-affinity binding to MFAP4 efficiently reduces pathological vascular responses *in vivo* in independent animal models of retinopathy. Our data support that MFAP4 has potential to serve as target and that hAS0326 constitutes a potential drug candidate for the treatment of vision-threatening retinal diseases characterized with vascular leakage and neovascularization, DME, and nAMD.

MATERIALS AND METHODS

Buffers

Tris-buffered saline (TBS): 140 mM NaCl (Merck Millipore), 10 mM Tris-HCl (Sigma-Aldrich), 0.02% (w/v) NaN_3 (Sigma-Aldrich), pH 7.4. TBS/Tw: TBS containing 0.05% (v/v) Tween 20 (polyoxyethylene sorbitan monolaurate, Merck Millipore). Phosphate-buffered saline (PBS): 137 mM NaCl (Merck Millipore), 3 mM KCl (Merck Millipore), 8 mM Na_2HPO_4 (VWR), 1.5 mM KH_2PO_4 (Merck Millipore), pH 7.4. PBS/Tw: PBS containing 0.05% (v/v) Tween 20 (polyoxyethylene sorbitan monolaurate, Merck Millipore). Substrate buffer: 35 mM citric acid (Sigma-Aldrich), 67 mM Na_2HPO_4 (VWR), pH 5.0. Fluorescence-activated cell sorting (FACS) buffer: PBS containing 0.5% BSA (Sigma-Alrich), 5 mM EDTA (Sigma-Aldrich). hAS0326 vehicle buffer: 10 mM histidine (Sigma-Alrich), 10% w/w trehalose (VWR chemicals), pH 6.0.

Single-cell transcriptome analysis

Spectacle (OcularGeneExpression.org/singlecell) is powered by cellcuratoR, an open-source R package.[45] Single-cell RNA sequencing expression data from the human retina and RPE/choroid were analyzed using Spectacle. Four publicly available human single-cell RNA sequencing datasets[45–49] consisting of 93,526 cells from a total of 19 human donors have been pre-processed with cellcuratoR for interactive visualizations with the Spectacle resource and were used for visualization of heatmap and dimensionality reduction.

Generation of mouse monoclonal antibodies

Recombinant human MFAP4 used for immunization was produced as previously described.[15] Monoclonal antibodies with affinity for MFAP4 were produced using standard hybridoma technique and MFAP4-deficient mice.[10] Generated antibodies included HG-HYB 7-5, HG-HYB 7-14, HG-HYB 7-18, and mAS0326.

Collection of vitreous from patients with retinal disease

Vitreous samples of patients with epiretinal gliosis, nAMD, and proliferative DR (Table S1) were collected by Dr. M. Koss, University of Heidelberg.[50] Exclusion criteria were previous intraocular surgery, acute ocular infection, uveitis, trauma, and retinal detachment. Samples were stored at −70°C. A total of 60 samples were collected; however, one sample obtained from patient with epiretinal gliosis, and one sample obtained from a patient with AMD, were excluded from the analysis due to insufficient material.

Measurement of MFAP4 in patient vitreous

Detection of MFAP4 was performed by AlphaLISA using two monoclonal anti-MFAP4 antibodies: biotinylated HG-HYB 7-18 and HG-HYB 7-14 conjugated to acceptor beads. The experiments were performed in duplicates and sample covariance was accepted if $\leq$10%. Determination of MFAP4 concentrations by AlphaLISA has been described in detail elsewhere.[12]

Patient eye samples used for *in situ* hybridization and immunohistochemistry

The 4-μm-thick sections of formalin-fixed, paraffin-embedded human eye tissues were retrieved from the tissue bank of the Eye Pathology Institute, University of Copenhagen. All patients had enucleation carried out because of pain. Eyes with AMD (n = 3) showed histological presence of serous subretinal neovascular membrane and/or a subretinal hemorrhage and/or a periretinal fibrous scar. Patients with DR (n = 5) all had a diabetes duration >10 years and all had received laser photocoagulation. All had proliferative diabetic retinopathy according to the International Clinical Diabetic Retinopathy Severity Scale outlined by the American Academy of Ophthalmology.[51] Moreover, all patients in the DR group were classified to be in advanced stages of DR. Four patients were diagnosed with proliferative diabetic retinopathy due to the presence of advanced neovascularization in the retina, and two patients showed signs of macular edema as well as advanced DR. The control group consisted of patients (n = 4) whose eye had been enucleated due to extraocular (orbital) cancer treatment. These eyes were clinically and histologically classified as normal, and none of the patients received radiotherapy.

Immunohistochemical detection of MFAP4

Anti-MFAP4 (HG-HYB 7-14), humanized anti-MFAP4 (hAS0326), and isotype control anti-OVA (HYB099-1, Staten Serum Institute, Copenhagen, Denmark) antibodies were labeled with fluorescein isothiocyanate (FITC) (isomer 1; Sigma-Aldrich, Saint Louis, MO) according to manufacturer's instructions. 4-μm-thick sections were cut from formalin-fixed, paraffin-embedded tissue blocks. Sections were mounted on FLEX IHC Slides (Dako; Glostrup, Denmark), dried at 60°C, dewaxed, rehydrated through a graded ethanol series, and subsequently washed in 0.05 M TBS (Fagron Nordic; Copenhagen, Denmark). Epitope retrieval was performed by protease treatment (0.05% protease type XIV; Sigma-Aldrich, St Louis, MO) for 15 min. The FITC-labeled antibodies were diluted to 2.5 μg/mL in antibody diluent (Agilent Technologies; Glostrup, Denmark). Incubation with the antibodies was done for 60 min at room temperature followed by incubation with anti-FITC-horseradish peroxidase (HRP) (Dako, Glostrup, Denmark, catalog [cat.] # P510050-8), diluted 1:30, for 20 min, and then using the DISCOVERY Purple kit (Roche cat. # 760-229) as HRP-driven chromogen. Immunostaining was followed by brief nuclear counterstaining in Mayer's hematoxylin-eosin (Fagron Nordic; Copenhagen, Denmark). Finally, slides were washed, dehydrated, and coverslipped using a Tissue-Tek Film coverslipper (Sakura Finetek; Alphen aan den Rijn, the Netherlands).

Positive and negative controls for immunostaining of MFAP4 using antibody HG-HYB 7-14 was previously shown using *Mfap4*$^{+/+}$ and *Mfap4*$^{-/-}$ mouse tissue, and similar staining pattern using HG-HYB 7-14 in human arteries was also previously demonstrated.[10,12]

In situ hybridization

RNA *in situ* hybridization (ISH) was conducted on human eye sections essentially as described in Lassen et al.[52] using a modified version of the RNAScope 2.5 high-definition procedure (322300, Advanced Cell Diagnostics [ACD] Bioscience, Newark, CA). Formalin-fixed, paraffin-embedded human eye sections with AMD or DR (described above) were used. 4-μm-thick sections were *in situ* hybridized with 20 probe pairs (571221, ACD) targeting nucleotides 109–1,150 of human MFAP4 mRNA (NM_002404.2) followed by branched-DNA signal amplification and tyramide-enhancement visualized with Liquid Permanent Red (K0640; Agilent). Negative controls were hybridized with probe diluent.

Western blotting of human retinas

Frozen (−80°C) retinal tissues were provided by Lions VisionGift, Portland, OR. The retinal tissues were obtained from two single eyes (two donors) without any eye disease. Data are shown from a 67-year-old Caucasian woman. Retinal tissue was homogenized using Precellys Tissue Homogenizer (Bertin Instruments) in ice-cold radioimmunoprecipitation buffer (RIPA) buffer (Sigma-Aldrich) supplemented with a cOmplete protease inhibitor cocktail tablet (Roche).

Retinal lysate supernatants were loaded onto a Criterion XT precasted 4%–12% Bis-Tris polyacrylamide gel (Bio-Rad) and electrophoresis was performed using the Criterion system (Bio-Rad) before standard western blotting using HG-HYB 7-5 anti-MFAP4 primary antibody (0.5 μg/mL) and HRP-conjugated rabbit anti-mouse Ig (Dako, cat. # P026002-2) secondary antibody (1:10,000). Proteins were detected using enhanced chemiluminescence reagents (Thermo Fisher Scientific).

Antibody humanization

mAS0326 antibody was humanized by GenScript (www.Genscript.com) using proprietary technology. Variable domain sequences were blasted against human germline and several framework regions FR1, FR2, and FR3 were selected independently from human framework regions (FRs) that share the highest identity with the mouse antibody. Selected FRs were assembled with mAS0326 CDRs using overlapping PCR, and phage display library was constructed for expression of Fab fragments. High MFAP4 protein-binding phages were selected after three rounds of panning using GenScript's proprietary FASEBA screening methodology. Selected Fab genes were amplified from phage DNA. Genes encoding Fab were fused with genes encoding the appropriate constant regions of human IgG1 to generate whole IgG. hAS0326 was selected as the best MFAP4 binder in this series using Biacore T200 and the resulting light-chain and heavy-chain constructs were cloned into the mammalian expression vectors pcDNA3.1 plus.

Expression of hAS0326

hAS0326 was transiently expressed in ExpiCHO-S cells. ExpiCHO-S cells (lot nr.1882582) were cultured in ExpiCHO expression medium in a shaker incubator set at 125 rpm, 37°C, and 8.0% CO_2 until reaching a cell density of 6×10^6 cells/mL. The day before transfection, ExpiCHO-S cells were diluted to 3.5×10^6 per mL in ExpiCHO expression medium. The hAS0326 light chain and hAS0326 heavy chain (produced by GenScript) were co-transfected in a molar 1:1 ratio using ExpiFectamine according to the manufacturer's protocol.

Before transfection, the cells were diluted to 6×10^6 cells/mL in ExpiCHO expression medium and then transfected using a total of 0.8 μg plasmid/mL of ExpiCHO-S cells. One day post transfection, ExpiCHO feed and ExpiCHO enhancer were added according to the manufacturer's protocol and the cells were transferred to a shaker incubator set at 125 rpm, 32°C, and 5.0% CO_2. Five days post transfection, ExpiCHO feed was added according to the manufacturer's protocol and, on day 12 post transfection, the culture supernatant was harvested by centrifugation at 10.000 ×g for 30 min. Cells and reagents were all from Thermo Fisher Scientific.

Purification of mAS0326

mAS0326 purification from hybridoma culture supernatant was performed by affinity chromatography using a protein G column as previously described.[53]

Purification of hAS0326

The ExpiCHO supernatant was filtered using a 0.22 μm filter (Millipore). The supernatant was then applied to serial-connected (3 × 5 mL) protein A Hitrap columns (GE Healthcare) using an Äkta Pure fast protein liquid chromatography (FPLC) apparatus (GE Healthcare), the column was washed in 10 column volumes of wash buffer (25 mM Tris and 25 mM NaCl, pH 7.2), and bound protein eluted in 100 mM citric acid with 100 mM NaCl, pH 3.5. As a viral inactivation step, hAS0326 was left for 30 min before adjustment to pH 5 using 1 M Tris, pH 8.6 buffer.

Cation exchange chromatography was performed using a 5 mL Capto S Hitrap column (GE Healthcare) and 100 mM phosphate pH 5.8 as a binding/wash buffer and then eluted using NaCl gradient over 20 column volumes (0–500 mM NaCl, 100 mM phosphate, pH 5.8). The eluted protein was dialyzed into 25 mM phosphate, pH 7.5 buffer before being applied to an anion-exchange chromatography column (5 mL Capto Q Hitrap column, GE Healthcare). The flow-through was collected and dialyzed into the formulation buffer (10 mM histidine [Sigma-Aldrich cat. # T9449], 10% w/v trehalose [VWR cat. # 3599.1000], and pH 6.0). Vivaspin 20 columns with a 30 kDa molecular-weight cutoff polyethersulfone (PES) membrane (Sartorius) were used to concentrate hAS0326 to a final concentration of 50 mg/mL. Endotoxin removal was subsequently performed using the NoEndo Standard column kit (Protein Ark) according to the manufacturer's instructions, and then the hAS0326 solution was sterile filtrated using 0.2 μm Q-Max PES syringe filter (Frisenette). The concentration of the hAS0326 solution was adjusted to 40 mg/mL and the endotoxin level of the final hAS0326 solution was tested using the Toxinsensor Chromogenic LAL endotoxin Assay Kit (GenScript) according to the manufacturer's instructions.

Purification of recombinant forms of MFAP4

For X-ray structure studies, recombinant MFAP4 protein was affinity purified as previously described.[54] For all other studies, recombinant MFAP4 was purified using antibody affinity chromatography as previously described.[10] Affinity chromatography was followed by anion ion-exchange chromatography on a Resource Q column (GE Healthcare Life Sciences) on an Äkta FPLC apparatus (GE Healthcare).

Biotinylation of antibodies

Antibodies were dialyzed against PBS adjusted to pH 8.5 with 3% (w/v) Na_2CO_3 (Sigma-Aldrich) and biotin-N-hydroxysuccinimide ester (Sigma-Aldrich H-1759, 40 mg/mL in dimethyl sulfoxide) was added at 0.17 mg/mg protein. The mixture was incubated overnight at 4°C and dialyzed against PBS.

Test of antibody binding to mouse recombinant MFAP4

96-well MaxiSorp plates (Nunc) were coated with 0.5 μg recombinant mouse MFAP4, human MFAP4, or MFAP4 variant with the amino acid RGD sequence mutated to AAA in PBS overnight at 4°C, washed, and blocked in TBS/Tw (tween) overnight at 4°C. The plate were then incubated with biotinylated detection antibodies: HG-HYB 7-5, mAS0326, or hAS0326 diluted 2-fold from an initial concentration of 100 ng/mL in TBS/Tw for 1 h at room temperature, washed in TBS/Tw, incubated with streptavidin-HRP conjugate (Invitrogen) diluted 1:2,000 in TBS/Tw for 20 min, washed again, and incubated with *o*-phenylenediamine dihydrochloride (OPD) substrate (0.8 mg/mL, Kementec) dissolved in substrate buffer (0.03% freshly prepared H_2O_2 [Sigma-Aldrich]) in the dark at room temperature. Color development was stopped by the addition of 100 μL of 1 M H_2SO_4, (Sigma-Aldrich) and the plates were read at OD_{492} nm with optical density 600 nm (OD_{600}) as reference.

Epitope mapping of antibodies by competition ELISA

96-well MaxiSorp plates (Nunc) were coated with 0.5 μg MFAP4 in PBS overnight at 4°C, washed, and blocked in TBS/Tw overnight at 4°C. Biotinylated mAS0326, hAS0326, or HG-HYB 7-5 (0.5 μg/mL) were premixed with single unlabeled monoclonal antibodies (mAbs) (isotype control, HG-HYB 7-5, HG-HYB 7-18, mAS0326, or hAS0326, diluted 2-fold from 20 μg/mL to 156 ng/mL) in a separate plate in TBS/Tw and added to the MFAP4-coated plate for 1 h at room temperature (RT). The plates were then washed in TBS/Tw, and biotinylated mAbs were detected using streptavidin-HRP conjugate (Invitrogen) as described above.

ELISA measuring the interaction between immobilized MFAP4 and integrins

96-well MaxiSorp plates (Nunc) plates were coated with 2 μg/mL recombinant human MFAP4 in PBS overnight at 4°C and washed with binding buffer (TBS/Tw supplemented with 0.1% BSA, 1 mM $CaCl_2$, 1 mM $MgCl_2$, and 1 mM $MnCl_2$). Soluble recombinant integrins $\alpha_v\beta_1$, $\alpha_5\beta_1$, $\alpha_v\beta_3$, $\alpha_v\beta_5$, $\alpha_v\beta_6$, $\alpha_v\beta_8$, $\alpha_{IIb}\beta_3$, $\alpha_4\beta_1$, and $\alpha_8\beta_1$ (all from R&D Systems) were diluted 2-fold in binding buffer and incubated in the coated wells for 2 h at RT. The plate was then washed with binding buffer and incubated for 1 h with biotinylated anti-α_v (cat. # BAF1219), anti-β_1 (cat. # BAF1778), or anti-β_3 (cat. # BAF2266) antibodies (all from R&D Systems) in binding buffer (0.5 μg/mL). Biotinylated mAbs were detected using streptavidin-HRP conjugate (Invitrogen) as described above.

IC50 estimation for hAS0326 Fab for inhibition of the interaction between integrin $\alpha_v\beta_3$ and MFAP4

96-well MaxiSorp plates (Nunc) were coated overnight at 4°C with recombinant human integrin $\alpha_v\beta_3$ (R&D Systems) in PBS, washed with binding buffer (TBS/Tw), and incubated for 1 h with 1.5 nM recombinant human MFAP4 and co-incubated with hAS0326 Fab fragments in 2-fold dilutions from 150 nM. The plates were then washed with binding buffer, incubated with biotinylated HG-HYB 7-18 for 1 h, and washed again. Biotinylated mAbs were detected using streptavidin-HRP conjugate (Invitrogen) as described above.

Sandwich ELISA for MFAP4 quantification in mouse serum

96-well MaxiSorp plates (Nunc) were coated with 1 μg/mL of anti-MFAP4 antibodies in PBS overnight at 4°C, washed in TBS/Tw, and blocked with TBS/Tw overnight at 4°C. The plates were then incubated with 2-fold dilutions of WT mouse serum or MFAP4-deficient mouse serum (initial dilution 1:50) overnight at 4°C, washed in TBS/Tw, incubated with biotinylated antibodies (0.5 μg/mL in TBS/Tw) for 2 h at RT, and washed again in TBS/Tw. Biotinylated mAbs were detected using streptavidin-HRP conjugate (Invitrogen) as described above.

Endotoxin test

Preparations of m/hAS0326 were tested for endotoxin contamination using limulus amebocyte lysate assay kit (GenScript) according to the manufacturer's instructions prior to use in cell cultures or animal experiments. All preparations of m/hAS0326 were below 1 EU (endotoxin units)/mL (*in vitro* and non-primate *in vivo* experiments) or below 0.2 EU/mL (NHP experiments).

Crystallization and structure determination

For Fab generation, hAS0326 was incubated with immobilized papain beads (Thermo Scientific) in 20 mM sodium phosphate, 10 mM EDTA, and 20 mM L-cysteine pH 7.4 for 4 h at 37°C. Beads were pelleted by centrifugation and the supernatant was loaded on a 1 mL Mono S column (GE Healthcare Life Sciences) equilibrated in 50 mM sodium acetate pH 5.5. The Fab was eluted with a gradient from 20 to 500 mM NaCl and subsequently purified by size-exclusion chromatography on a 24-mL Superdex 200 Increase column (GE Healthcare Life Sciences) equilibrated in 20 mM HEPES, 150 mM NaCl, pH 7.4. Prior to crystallization, MFAP4 was deglycosylated for 18 h at 4°C with in-house prepared endoglycosidase H. Deglycosylated MFAP4 was mixed with an excess of Fab and the complex was purified on a 24 mL Superdex 200 Increase column equilibrated in 20 mM HEPES pH 7.4, 150 mM NaCl. The isolated complex was concentrated to 6 mg/mL and crystallized by vapor diffusion at 19°C after mixing 0.5 μL of protein with 0.5 μL of reservoir solution containing 0.14 M ammonium phosphate dibasic, 14% w/v polyethylene glycol 3350 (Sigma-Aldrich). Prior to data collection, crystals were soaked in reservoir solution supplemented with 20% glycerol and flash-cooled in liquid nitrogen.

Diffraction data were collected at ESRF ID23-1 and processed and scaled with XDS and XSCALE.[55] The structure was determined by molecular replacement with Phenix.phaser[56] using the structure of monomeric fibrinogen C-containing 1 (FIBCD1) (PDB: 4M7H) and a germline Fab (PDB: 4JPI) as search models. In an iterative manner, the structure was manually rebuilt in Coot and refined with Phenix.refine[57] using positional refinement, grouped B-factors, TLS groups, and positional non-crystallographic symmetry restraints. Upon completion of the protein part of the model, the structure was fitted to the electron density map using molecular dynamics restrained real space fitting as previously described.[58] Subsequently, Ca^{2+} ions and two coordinating water molecules were inserted into each site, and the calcium-ligand coordination geometry was restrained according to that observed in FIBCD1.[18] During the final refinement cycles, a few cycles of individual B-factor refinement were allowed in addition to positional refinement. The stereochemistry was analyzed with Molprobity,[59] intermolecular interface was investigated with PyMol[60] and PISA,[61] and figures prepared in PyMol.

Experimental validation of the crystal structure

Five paratope residues in the MFAP4-hAS0326 interface were selected for experimental validation of the observed protein-protein interactions. DNA encoding hAS0326 Fab, hAS0326 W33A H-CDR1 Fab, hAS0326 S55A H-CDR2 Fab, hAS0326 H107A H-CDR3, hAS0326 Y32A L-CDR1 Fab, and hAS0326 Y94A L-CDR3 Fab were synthesized and inserted into pcDNA3.1+ plasmids by GenScript. The plasmids were co-transfected with the hAS0326 light-chain plasmid into ExpiCHO cells and expressed as previously described. The Fabs were following purified using protein L affinity chromatography followed by dialysis into PBS. Binding parameters of hAS0326 mAb and hAS0326 Fabs were determined by biolayer interferometry using an Octet RED96e system (Pall ForteBio) at 22°C, orbital sensor agitation at 1,000 rpm in 200 μL volume. First, streptavidin (SA) biosensors (#18-5020, Pall ForteBio) were pre-hydrated for 10 min in BLI running buffer (BLI-RB) (10 mM HEPES, 150 mM NaCl, 3mM $CaCl_2$, 0.05% Tween 20, 0.1% BSA, pH 7.4) followed by capture of biotinylated MFAP4 (36 kDa, 5 mg/mL in BLI-RB) until a loading of 1 nm was achieved. MFAP4 was biotinylated with an EZ-Link NHS-PEG_4-biotin (#21330, Thermo Fisher Scientific) by mixing in ratio 1:3 (MFAP4:biotin) and incubating for 30 min at RT. Baseline was generated in BLI-RB over 120 s. Association with different concentrations of Fab (55 kDa) or mAb (150 kDa) (diluted in BLI-RB) was measured for 1,000 s, and dissociation in BLI-RB was measured as well over 1,000 s. Loaded biosensor measurements in absence of Fab or mAb were used as reference and subtracted from all binding curves. Sensors were regenerated in 100 mM glycine, 1 M NaCl, pH 3 for 3 × 5 s. Sensorgrams were aligned using the last 5 s of baseline and fitted using 1:1 binding model (ForteBio Data Analysis 10.0 software) analyzing both association and dissociation. Binding curves were analyzed using global (full) fit with R_{max} unlinked by sensor. A Savitzky-Golay filter was applied to smoothen the data.

Tolerability of i.v.t. hAS0326 in rats

Studies were performed at EyeCRO (Oklahoma City, OK). Female brown Norway rats (>3 weeks old) weighing between 120 and 150 g were obtained from Charles River Laboratories (Wilmington,

MA, USA). A total of 11 animals were used. All animals were housed under standard animal care conditions. The animals were maintained under normal light cycle conditions consisting of 12 h of light (<500 lux) followed by 12 h of darkness. Animals were anesthetized with ketamine/xylazine and pupils were dilated with topical administration of Cyclogyl and/or tropicamide. Following sedation and dilation, a total volume of 5 μL of mAS0326 (60 μg in PBS pH 7.2) (n = 6) or PBS (pH 7.2) (n = 5) per eye was injected into the vitreous at the pars plana using a Hamilton syringe and a 33-gauge needle. The ocular surface and surrounding areas were examined once a day throughout the study. For Draize scoring of hyperemia, chemosis, and discharge, animals were restrained by hand and scores for chemosis, hyperemia, and discharge were recorded by a masked observer using the EyeCRO ocular scoring system (scoring 0–4). After a minimum 12 h of dark adaptation, animals were anesthetized by intraperitoneal injection of 85 mg/kg ketamine and 14 mg/kg xylazine. Animal preparation was performed under a dim red light (<50 lux). Electroretinography (ERG) analyses were performed using an Espion system from Diagnosys (Lowell, MA). For the assessment of scotopic response, a stimulus intensity of 40 (S) cd-s/m^2 was presented to the dark-adapted dilated eyes. The amplitude of the scotopic a-wave was measured from the pre-stimulus baseline to the a-wave trough. The amplitude of the b-wave was measured from the trough of the a-wave to the crest of the b-wave. To evaluate photopic response, animals were light adapted for 7 min, then presented a strobe flash to the dilated eyes with an intensity of 10 (S) cd-s/m^2. A total of 15 repeated flashes and measurements were averaged to produce the final waveform. The amplitude of the photopic b-wave was measured from the trough of the a-wave to the crest of the b-wave. On the beginning of any day of ERG, the response of WT C57Bl/6 mice ($n \geq 2$) was recorded and quantified to ensure proper device calibration. Animals were euthanized with a lethal dose of pentobarbital on day 22. Whole eyes were enucleated and fixed overnight in 4% paraformaldehyde. Eyes were cut into sections and stained with hematoxylin and eosin.

Cell culture

Immortalized HPMECs (ST1.6R) were kindly provided by R.E. Unger Johannes, Gutenburg University. Primary human RECs were obtained from Neuromics (Edina, MN, USA). Endothelial cells were grown in Endothelial Cell Growth Medium MV (PromoCell) supplemented with 50 U/mL penicillin and 50 μg/mL streptomycin (Gibco) and used between passages 2 and 10 in all *in vitro* experiments.

Flow cytometry

HPMECs were detached with Accutase (Fisher Scientific) and suspended at 200,000 cells/sample in FACS buffer containing 10 μg/mL mouse mAbs against integrin $\alpha_V\beta_3$ (Millipore, cat. # MAB1976), integrin $\alpha_V\beta_5$ (Santa Cruz, cat. # sc-13588), with anti-ovalbumin (HYB099-01), The State Serum Institute) as isotype control (IC) for 1 h at 4°C. Secondary antibody was polyclonal goat anti-mouse FITC-conjugated goat F(ab')2 (Dako, cat. # F0479). The analysis was performed using LSR II (BD Biosciences) flow cytometer and BD FACSDiva software (BD Biosciences). Obtained data were further analyzed using FlowJo software (Tree Star).

Adhesion assay

HPMEC adhesion to immobilized MFAP4 was assessed using the Vybrant Cell Adhesion Assay Kit (Molecular Probes, Invitrogen) according to the manufacturer's instructions. Briefly, a black 96-well plate (Nunc) was coated with MFAP4 or bovine or human serum albumin (Sigma-Aldrich) at 4°C overnight, washed with PBS, blocked with 10 mg/mL sterile BSA for 1 h at RT, and washed again. Calcein-labeled cell suspensions were loaded on to the pre-coated plate at 1–2 × 10^5 cells/well. In some experiments, the plate was incubated with 10 μg/mL mAS0326 or anti-ovalbumin IC (R&D Systems) for 1 h at RT, or, alternatively, calcein-labeled cells were pre-incubated with 25–100 μg/mL GRGDS integrin-blocking peptide or SDGRG control peptide (both from Sigma-Aldrich), or anti-integrin $\alpha_V\beta_3$ (Millipore, cat. # MAB1976), or anti-integrin $\alpha_V\beta_5$ (Santa Cruz, cat. # sc-13588) blocking antibody, or IC (HYB099-1, Staten Serum Institute, Copenhagen, Denmark) for 30 min at RT. After 1 h of incubation at 37°C, the plate was gently washed four times with warm medium and filled with 200 μL PBS. The fluorescence was measured at 485/535 nm using a VICTOR 3 multilabel plate reader (PerkinElmer). All samples were normalized to blank wells containing PBS only (Sigma-Aldrich).

Regulation of endothelial pFAK and pERK1/2 by MFAP4

Six-well tissue culture plates (Nunc) were coated with 20 μg/mL MFAP4, vitronectin (Sigma-Aldrich), or poly-D-lysine (Sigma-Aldrich) overnight at 4°C, washed with PBS, blocked with 10 mg/mL BSA for 1 h at RT, and washed again.

HPMECs were serum starved overnight in phenol red-free DMEM. Cells were detached with Accutase and incubated in phenol red-free DMEM containing 1% BSA (Sigma-Aldrich) for 1 h at 37°C. 500.000 cells/mL were seeded and allowed to adhere for 10, 20, 40, 60, or 120 min. Next, the cells were lysed with ice-cold RIPA buffer (Sigma-Aldrich) supplemented with a cOmplete protease inhibitor cocktail tablet (Roche) and 0.001% phosphatase inhibitor sodium orthovanadate (Na_3VO_4) (Sigma-Aldrich) for 45 min at 4°C while shaking.

Cell lysates were loaded onto a Criterion XT pre-casted 4%–12% Bis-Tris polyacrylamide gel (Bio-Rad), and electrophoresis was performed using the Criterion system (Bio-Rad) before standard western blotting using rabbit mAbs against phospho-p44/p42 MAPK (ERK1/2) (Thr202/Tyr204) (clone 20G11, cat. # 4375), p44/p42 MAPK (ERK1/2) (clone 137F5, cat. # 4695), phospho-Akt (Thr308) (clone 244F9, cat. # 4096), and pan-Akt (clone 11E7, cat. # 4685); rabbit polyclonal antibodies against phospho-FAK (Tyr397, cat. # 3283) and FAK (cat. # 3285) (all from cell Signaling); and a mouse polyclonal antibody against GAPDH (Santa Cruz, cat. # sc-47724). All primary antibodies were diluted 1:1,000. Secondary antibodies were HRP-conjugated goat anti-rabbit Ig (Dako cat. # PO44801-2) or HRP-conjugated rabbit anti-mouse Ig (Dako, cat. # PO26002-2). Proteins were detected using enhanced chemiluminescence reagents.

Proliferation assay

A 96-well plate was pre-coated with MFAP4, washed, and blocked as described above. Serum-starved RECs were seeded (20,000 cells/well) in MFAP4-coated wells and incubated in Endothelial Cell Basal Medium (PromoCell) for 24 h at 37°C. The cells were allowed to adhere for 3 h. The cells were then treated with hAS0326, anti-integrin $\alpha_V\beta_3$ (Millipore, cat. # MAB1976), anti-integrin $\alpha_V\beta_5$ (Santa Cruz, cat. # sc-13588), or IC (HYB099-1, Staten Serum Institute, Copenhagen, Denmark) antibody for 1 h before and throughout stimulation with 100 ng/mL VEGF (recombinant human VEGF-A R&D Systems). The next day, the cells were stained with 1 mg/mL MTT (MTT assay, Thermo Fischer Scientific) for 4 h, after which the medium was removed and the plate was incubated in isopropanol containing 0.1 M HCl for 15 min at RT with shaking. The absorbance was then read at 592 nm vs. 620 nm.

Migration assay

The lower side of the Transwell inserts with 8.0 μm pores (Corning) was coated with 10 μg/cm^2 MFAP4 or albumin overnight at 4°C and washed with PBS. REC were collected, resuspended in Endothelial Cell Basal Medium (PromoCell) containing 0.5% FBS (Thermo Fisher), and seeded in the upper chamber of the inserts (50,000 cells/insert). Lower chamber contained Endothelial Cell Basal Medium with 0.5% FBS ± 25 ng/mL VEGF (RECs). In some samples 10 μg/mL hAS0326 antibody was added to the lower chamber. Alternatively, anti-integrin $\alpha_V\beta_3$, anti-integrin $\alpha_V\beta_5$ (both from R&D Systems), or anti-ovalbumin IC antibody were added to the upper chamber when seeding the cells. The cells were allowed to migrate for 3.5 h (RECs), after which the upper sides of the filters were washed with PBS and swiped with a cotton swab to remove any non-migrated cells. The lower sides of the filters were stained with Hemacolor (Sigma-Aldrich) and divided into four fields. The cells in each field were counted in a blinded manner by two independent observers.

Murine laser-induced CNV model

CNV was induced and analyzed essentially as described previously.[62] Female C57BL/6J mice (Charles River Laboratories International, 6–8 weeks old) were anesthetized with an intraperitoneal injection of 50 mg/kg Ketaset (ketamine hydrochloride, Zoetis), and recovered with 0.5 mg/kg intraperitoneal Sedastop (atipamezole hydrochloride, Animalcare). Pupils were dilated with topical applications of 5% phenylephrine hydrochloride (Bausch & Lomb) and 0.8% tropicamide (Bausch & Lomb), and eyes were coated with Lubrithal (Dechra) to prevent dehydration.

Right-eye lesions were produced using a Meridian Merilas 532α Green Laser Photocoagulator (Phoenix Technology Group) to penetrate the Bruch's membrane at four points per eye in both eyes. The presence of a subretinal bubble was used to determine the successful rupture of the Bruch's membrane. Laser settings were maintained at 450 mW for 130 ms for each photocoagulation lesion.

Mice received an intraocular injection of 1 μg of hAS0326, 5 μg of hAS0326, saline as negative control, or 1 μg of neutralizing anti-VEGF-A (Ultra-Leaf purified anti-Mouse VEGF-A antibody, Biolegend, cat. # 512809) as positive control. Antibodies were diluted to 0.5 μg/μL (2.5 μg/μL for 5 μg injections) in sterile PBS and 2 μL was administered with a 36-gauge Hamilton needle (World Precision Instruments) with fine forceps used to stabilize the eye. Antibodies were administered on day 0 (post lesion) and day 7.

To visualize the vasculature and lesion development *in vivo* (day 14), 200 μL of 100 mg/mL sodium fluorescein (Sigma-Aldrich) in saline was injected intraperitoneally and allowed to circulate before imaging with a Micron IV retinal imaging microscope (Phoenix Research Labs) as previously described.[62] Circulation of fluorescein was routinely imaged 1 min after injection. Development of cataracts meant that some eyes were excluded from the consecutive FFA. One eye from the anti-VEGF treatment group and one from the 1 μg hAS0326 treatment group were excluded.

After animal termination and ocular dissection (day 14), choroids were flat mounted and blocked in serum (5% goat serum [Abcam], 3% Triton X-100 [Sigma-Aldrich], 1% BSA [Fitzgerald Industries International]) and stained with isolectin-B4 (IB4) (Sigma-Aldrich, biotin conjugated) (5 μg/mL) overnight at 4°C. Streptavidin-conjugated Alexa Fluor 488 (Thermo Fisher Scientific) (2 μg/mL) and donkey anti-rabbit Alexa Fluor 555 (Thermo Fisher Scientific, cat. # A-31572) (4 μg/mL) were used for detection. Coverslips were mounted with Fluoroshield (Vector Laboratories) with DAPI. Images were obtained using a Leica TCS SPE confocal microscope (Leica Biosystems), and all settings were maintained between images. Lesion and inflammatory cell volumes were measured directly by Imaris (Bitplane, UK). Any lesions that had merged, or animals in which the contralateral eye had burns measuring greater than 2 standard deviations from the mean, were excluded from analysis.

Rat STZ-induced diabetes model

Male Norway brown rats (250–300 g, Envigo, US) were weighed and administered a single intraperitoneal injection of STZ (50 mg/kg, Sigma-Aldrich, MO, USA). Control rats were administered with 250–300 μL saline depending on their individual starting weight. On day 3, a third of an insulin capsule (LinShin, ON, Canada) was implanted subcutaneously to maintain body weight over the 21-day study. On day 4 post induction, tail vein blood was sampled, and glucose levels were measured using an Accu-Chek glucose meter (Roche, UK). Rats with blood glucose levels of 15 mmol/L and above were deemed diabetic.

Rats were anesthetized with 3%–5% isoflurane (IsoFlo, Abbott Laboratories, UK), pupils dilated with topical application of 5% phenylephrine hydrochloride (Bausch & Lomb, UK) and 0.8% tropicamide (Bausch & Lomb, UK), and eyes coated with a drop of Lubrithal (Dechra UK) to prevent dehydration. Animals received a right-eye intraocular injection of 1 μg m/hAS0326, 5 μg m/hAS0326, 1 μg rabbit anti-VEGF-A (Abcam, Cambridge, UK, cat. # ab9570), or saline as negative control. Antibodies were diluted to 0.5 μg/μL (2.5 μg/μL for 5 μg injections) in sterile PBS and 2 μL administered with a

36-gauge Hamilton needle (World Precision Instruments, FL, USA) with fine forceps used to stabilize the eye. Antibodies were administered on day 0 (pre-diabetic) and day 7 (post diabetic). To visualize the vasculature and lesion development *in vivo* (day 0, 7, 14, and 21), 200 μL of 100 mg/mL sodium fluorescein (Sigma-Aldrich, MO, USA) in saline was injected intraperitoneally and the retina was imaged from the point of injection for 3 min using a Micron IV retinal imaging microscope (Phoenix Technology Group, CA, USA). On day 14, four eyes were excluded due to development of corneal opacity, and one eye was excluded due to the fluorescein being injected into the gut by mistake and being rapidly cleared.

Retinal permeability analysis

This model was performed essentially as previously.[63] In short, angiograms were imported into ImageJ software and fluorescence was measured in the interstitium and in a major retinal vessel every 200 frames up to 2,400 frames. The ratio of interstitial to vascular fluorescence was adjusted for background level and plotted against time. The permeability coefficient (permeability × surface area product) was calculated from the rate of change of extravascular fluorescence ($=\Delta I_f/\Delta t$) per unit concentration difference (ΔC):permeability coefficient = $\Delta I_f/\Delta t/(\Delta C \times A)$.

Immunohistochemical detection of hAS0326 in rabbit eyes

New Zealand white (NZW) female rabbits (2.2–2.5 kg) (Envigo, UK) received 50 μL of i.v.t. hAS0326 40 mg/mL or vehicle (10 mM histidine, 10% trehalose, pH 6) (n = 3/group). Animals were culled and eyes were enucleated after 1 week and fixed in 4% formaldehyde. hAS0326 was detected by immunohistochemistry. 4-μm-thick sections were cut and mounted on FLEX IHC microscope slides (Dako/Agilent, Glostrup, Denmark). Sections were dried at RT and baked at 60°C for 60 min before immunostaining. Staining was automated at the Discovery Ultra immunostainer (Ventana Medical Systems, Tucson, AZ) using the OmniMap anti-goat-HRP detection system (Ventana Medical Systems, Tucson, AZ) and DISCOVERY Purple chromogen kit (Ventana Medical Systems, Tucson, AZ). Incubation with goat anti-human IgG Fc (Abcam, Cambridge, UK, cat. # 97221) diluted 1:2,000, was done for 32 min at 36°C. Epitope retrieval was performed in Cell Conditioning Solution 1 (CC1) for 32 min at 100°C. Nuclear counterstaining was performed using hematoxylin II (Ventana Medical Systems, Tucson, AZ). Finally, slides were washed, dehydrated, and coverslipped using an automated Dako coverslipper (Dako/Agilent, Glostrup, Denmark).

NHP studies

Adult African green monkeys of mixed sex and age were used. The animals were collected and studied in Virscio examination and procedure room located on the St. Kitts Biomedical Research Foundation campus, Lower Bourryeau Estate, St. Kitts, West Indies. Monkeys were either purpose bred at the facility or captured humanely from the feral population on the island of St. Kitts. Monkeys were individually housed in 3 × 2.6 × 2 ft squeeze cages in free-standing enclosures exposed to ambient environmental conditions, which approximated a 12:12 h light-dark cycle with temperatures between 20.0°C and 34.9°C and humidity range of 52%–99%. All monkeys were fed pelleted monkey chow biscuits (Harlan Teklad, Madison, WI, crude protein = 20%, crude fat = 5%, crude fiber = 10%) *ad libitum*.

Tolerability of i.v.t. hAS0326 in NHP

Healthy adult male (n = 24) and female (n = 24) African green monkeys (2.16–6.15 kg) were enrolled in the study. After baseline ophthalmic examinations, including tonometry, slit lamp biomicroscopy, fundoscopy, color fundus photography, FFA, and optical coherence tomography, 12 monkeys with normal findings were enrolled in the study and randomized by sex and baseline body weight into four treatment groups receiving either vehicle (10 mM histidine, 10% trehalose, pH 6.0), 0.5 mg, 1.25 mg, or 2 mg hAS0326 in 50 μL in both eyes. Animals were sedated by intramuscular injection of ketamine/xylazine (8 mg/kg/1.6 mg/kg) for examination and treatment procedures. For i.v.t. dosing, topical local anesthesia was administered (0.5% proparacaine) and eyes disinfected with 5% Betadine and rinsed with 0.9% sodium chloride. i.v.t. injections were administered with a 0.3 mL insulin syringe with a 31-gauge 5/16-inch needle placed ∼2.5 mm posterior to the limbus in the inferior temporal quadrant, targeting the central vitreous. A topical antibiotic ointment (neomycin/polymyxin B sulfates/bacitracin zinc) was administered after the injection. General well-being was confirmed twice daily by cage side observations beginning 1 week prior to dosing. Daily individual food consumption was assessed by visual inspection of the feed pan or cage floor prior to cage washing following routine feeding for overall appetite. Monkeys were subjected to tonometry and slit lamp exams on days 2, 7, and 14 and to color fundus photography (CFP), FFA, and optical coherence tomography (OCT) on days 7 and 14 after dosing. CFP, FFA, and OCT were performed essentially as described previously.[64] Following completion of specified exams and confirmation of good ocular and overall health, the monkeys were returned to the colony.

NHP DL-AAA-induced model of chronic retinopathy

Healthy adult male and female African green monkeys (3.05–6.33 kg) were enrolled in the study. Enrolled monkeys received i.v.t. injections of DL-AAA (5 mg/200 μL, Sigma-Aldrich product code A0637) in both eyes on day 0 and the leakage development was followed using angiography as previously described.[22] The dose of DL-AAA was reduced to 3.75 mg/100 μL in a few animals to titrate the induced retinal pathology associated with a new batch of DL-AAA (Table S4).

At week 10 following DL-AAA treatment, fluorescein angiography images were graded by a masked assessor to evaluate severity of DL-AAA-induced retinal leakage, referencing a standard leakage size scoring scale.[22] Eyes from enrolled animals were stratified based on leakage size scores and assigned to treatment groups to achieve balanced severity of baseline DL-AAA-induced pathology.

One i.v.t. injection of vehicle, 2 mg hAS0326, or 0.5 mg ranibizumab (Novartis, batch SMT739) in 50 μL was provided as described above in week 10. Animals were following examined by FFA in weeks 12, 13,

14, 16, 18, 20, and 22. Vitreous taps were performed at week 0, 10, 14, and 22.

Leak area measurements were performed on individual eyes from week 8 through week 22 (post DL-AAA). There were a minimum of five animals in each group, but, in some groups, both eyes were enrolled. Early-phase (1 min) fluorescein angiography images of the macula that fully covered the lesion area were exported from the Heidelberg software (HEYEX) as tiff files and imported to Adobe Photoshop CC (Adobe Systems, San Jose, CA, USA). Leakage area was quantified by an examiner masked to treatment by tracing over the fluorescein cloud on the surface of the retina using a paintbrush tool and calculating the number of pixels covered. Leakage area from each image was standardized using the area of the optic nerve head in the same image. Inclusion criteria for the angiogram images were the following: lesion fits on a single image; fluorescein cloud has clear borders; there are no RPE windows, retinal detachments, or cataracts.

Measurement of MFAP4 in NHP vitreous

Vitreous was diluted 1:50 and measured essentially as described in Sækmose et al. 2013,[15] with the exception that the HG-HYB 7-5 catcher antibody was used as full-length antibody instead of as F(ab')2.

Proteomic analysis

Macular punches including choroid, RPE, and retina were obtained at end-study (week 22) from the DL-AAA-induced retinopathy study in NHP. The punches were manually ground using pestles for homogenization (Scientific Specialities, USA) in ice-cold RIPA buffer (Sigma-Aldrich) supplemented with a cOmplete protease inhibitor cocktail tablet (Roche) and phosphatase inhibitor PhosphoSTOP (Roche). Protein lysates (10 μg per sample) from NHP macular punches were reduced in the presence of 5 mM dithiothretiol (DDT) at 50°C for 30 min followed by alkylation by iodoacetamide (15 mM, 30 min in the dark). Reduced and alkylated proteins were precipitated by acetone precipitation, re-dissolved in 0.2 M triethyl ammonium bicarbonate, and incubated with 1/50 w/w trypsin overnight at 37°C. The resulting tryptic peptide samples were labeled using the 16-plex tandem mass tag (TMTpro, Thermo Fisher Scientific, Waltham, MA, USA) where a pool of all samples were labeled with the mass tag 126, which served as an internal standard. Tagged peptides were mixed into two mixed peptide samples that were fractionated into eight fractions using high-pH chromatography. Samples were loaded onto an ACQUITY UPLC M-Class CSH C18 column (130 Å, 1.7 μm bead size, 300 μm inside diameter [ID] × 100 mm length) using a linear gradient from 10% solvent B (20 mM ammonium formate in 80% acetonitrile [ACN], pH 9.3) to 55% solvent using a 25 min linear gradient at 6 μL/min flowrate on a Dionex Ultimate 3000 RSLnano system inline coupled to a Dionex 3000 ultimate UV detector and a Dionex Ultimate 3000 autosampler configured as a fraction collector.

Nano-liquid chromatography-tandem mass spectrometry (LC-MS/MS) analysis of fractionated samples was conducted on an Orbitrap Exploris mass spectrometer (Thermo Fisher Scientific, Bremen, Germany) equipped with a FAIMS Pro interface (Thermo Fischer Scientific, Slangerup, Denmark) coupled with a nano-high-performance liquid chromatography (HPLC) interface (Dionex UltiMate 3000 nano HPLC). The samples (5 μL) were loaded onto a custom-made fused capillary pre-column (2 cm length, 360 μm outside diameter [OD], 75 μm ID packed with ReproSil Pur C18 3 μm resin (Dr Maish)) with a flow of 5 μL/min for 6 min. Trapped peptides were separated on a custom-made fused capillary column (25 cm length, 360 μm OD, 75 μm ID, packed with ReporSil Pur C13 1.9 μm resin) using linear gradient ranging from 91% to 86% solution A (0.1% formic acid) to 25%–34% B (80% ACN in 0.1% formic acid) over 100 min followed by 5 min at 90% B and 5 min at 98% A at a flow rate of 250 nL per minute.

Mass spectra were acquired in positive-ion mode applying automatic data-dependent switch between an Orbitrap survey MS scan in the mass range of 400–1,400 *m/z* followed by peptide fragmentation applying a normalized collisional energy of 38% in a 3 s duty cycle and by switching the FAIMS unit between CVs of −50 V and −70 V with a 2 s cycle time. Target value in the Orbitrap for MS scan was set to 1E6 ions at a resolution of 60,000 at *m/z* 200 and 2E5 ions at a resolution of 45,000 at *m/z* 200 for MS/MS scans. Ion selection threshold was set to 1E4 counts. Selected sequenced ions were dynamically excluded for 60 s.

All Exploris raw data files were processed and quantified using Proteome Discoverer version 2.4 (Thermo Scientific, Waltham, MA, United States) applied TMTpro (N terminus and lysine) and cysteine carbamidomethylation as fixed modifications and methionine oxidation and asparagine and glutamine deamidation as fixed modifications. Data were searched against the UniProt Green monkey_60711 protein database (19,711 entries, downloaded May 11 2023).

5,122 unique proteins were identified. Pathway enrichment analyses were performed using clusterProfiler 4.0 package[65] and org.Hs.eg.db in R based on ranked log2-transformed fold changes (gse function) and unadjusted $p < 0.05$ (unpaired, two-tailed student's t test for each protein per two-group comparison) (compareCluster function), respectively. In both analyses, the Benjamini-Hochberg procedure was applied to correct for multiple testing.

Western blotting of NHP macular punches

Protein lysates as described above for proteome analysis were also used for this analysis. Lysates were analyzed by western blotting using the XCell II Blot Module and the NuPAGE electrophoresis system (Invitrogen by Life Technologies) according to the manufacturers technical guide. Antibodies applied for detection of MFAP4 included HG-Hyb 7-5 mouse mAb, with blocking in TBST + 5% non-fat dry milk (Bio-Rad). The secondary antibody was Rabbit-anti-Mouse (Dako, cat. # P0448). Antibodies applied for detection of integrins included rabbit anti-integrin α_V mAb (EPR16800) (Abcam, cat. # ab179475), rabbit anti-integrin β_3 antibody (D7X3P) XP mAb (Cell Signaling, cat. # 13166), and rabbit anti-integrin β_5

antibody (D24A5) mAb (Cell Signaling, cat. # 3629). The secondary antibody was Goat-anti-Rabbit (Dako, cat. # P0260). Blocking was performed in Roti-Block (Carl Roth, cat. # A151.1). Proteins were detected using SuperSignal Chemiluminescent S (Thermo Fisher Scientific) using ChemiDoc MP imaging system (Bio-Rad) and Image Lab 6 software. Band intensity was quantified using ImageJ software (imagej.net).

Pharmacokinetics of i.v.t. hAS0326 in NHPs

Healthy adult male (n = 11) and female (n = 8) African green monkeys (2.48–6.02 kg) were enrolled in the study. Baseline screening included tonometry, slit lamp biomicroscopy, and fundoscopy. For i.v.t. dosing, a drop of proparacaine hydrochloride 0.5% was placed in the eye followed by a lid speculum, then 5% Betadine solution, and a rinse with sterile saline. i.v.t. injections were administered using 0.3 mL insulin syringe with a 31-gauge 5/16-inch needle (Ulticare VetRx U-100) placed ∼2.5 mm posterior to the limbus in the inferior temporal quadrant, targeting the central vitreous. A topical antibiotic ointment (neomycin/polymyxin B sulfates/bacitracin zinc) was administered after the injection. hAS0326 was administered i.v.t. at dosage of 2 mg/eye in both eyes in 50 µL; n = 3 animals per time point. One animal received no treatment. Following hAS0326 administration, one eye was fixed and one eye was freshly dissected from each animal. Samples were taken at 24 h and 3, 7, 14, 35, and 63 days post dose. At each time point, each group of monkeys were euthanized with intravenous sodium pentobarbital (100–120 mg/kg to effect) at designated time points. The left eye was freshly dissected to remove the anterior segment of the eye. After collection and flash-freezing of all remaining vitreous humor (1 mL × 2 aliquots), the eyecup was flattened by applying four longitudinal cuts to create superior, nasal, inferior, and temporal petals radiating from the central macular region with the choroid + sclera + retina intact in each region. Retina/RPE/choroid were collected together into pre-tared, pre-labeled vials, weighed, and flash-frozen in liquid nitrogen. All frozen samples were stored at −70°C until analysis.

ELISA detection of free hAS0326 in vitreous humor and retinal/choroid tissue

96-well MaxiSorp plates (Nunc MaxiSorp) were coated with MFAP4 (0.25 µg/mL in PBS) overnight at 4°C, washed with PBS/Tw/BSA, and then blocked with PBS/Tw for 1 h at RT. To create a standard curve, hAS0326 was diluted to 10 ng/mL in PBS/Tw/BSA, followed by 2-fold dilutions in PBS/Tw/BSA. Vitreous samples were homogenized by flushing twice through a 1 mL syringe and thereafter three to five times through a 1 mL syringe fitted with an 18-gauge × 1–1.5-inch needle until the ECM was broken. The vitreous fluid was centrifuged for 5 min at 12,000 × g at 4°C. Retina/choroid tissue homogenized in RIPA buffer (Sigma-Aldrich cat. # R0278) using a Precellys 24 tissue homogenizer (Bertin Instruments) were diluted with PBS/Tw/BSA to be within the linear range of the assay and aliquoted onto the MFAP4-coated plates (100 µL per well). All samples were incubated for 1 h at RT, washed with PBS/Tw/BSA, and incubated with HRP-conjugated goat anti-human IgG (Abcam, cat. # ab97225) at 1:10,000 dilution in PBS/Tw/BSA for 30 min at RT. The plates were then washed and incubated with HRP substrate in the dark for 15 min at RT. The reaction was stopped with 1 M H_2SO_4. The absorbance at 492 nm and 650 (reference) was measured with a microplate reader.

Statistical analysis

Statistical analysis was performed using Stata/IC 15.0 (Statanordic), Prism 7, and/or Prism 9 (https://www.graphpad.com). Comparison between clinical vitreal MFAP4 levels was performed using Kruskal-Wallis test. The level or frequency of MFAP4, sex, age, central retinal thickness, previous intravitreal injection, and previous core pars plana were compared in groups of patients with epiretinal gliosis, nAMD, and pDR using one-way ANOVA followed by Tukey's or Dunnett's multiple comparisons test. Subgroups of nAMD were compared separately, but no significant differences were found. *In vitro* data were analyzed using two-way or one-way ANOVA or mixed-effects model (in case of missing data) followed by Tukey's, Dunnett's, or Šidák multiple comparisons test.

Comparisons between treatment groups in rodent experiments were performed using one-way ANOVA followed by Dunnett's multiple comparison tests. Mixed-effects model followed by Dunnett's multiple comparisons test was used to compare vitreous MFAP4 levels relative to week 0. Mixed-effects analysis with repeated measures followed by Dunnett's multiple comparisons test was performed to evaluate significant overall therapeutic effects of individual treatments relative to pre-dose FFA intensity measured at week 10 in non-human-primate DL-AAA-induced model of chronic retinopathy. One-way ANOVA followed by Tukey's multiple comparisons test was used to compare treatment efficacy of vehicle, hAS0326, or ranibizumab at a single time point (week 12 or week 22). Multiple linear regression was following performed with either week 12 or week 22 treatment effect as the dependent variable and the covariates treatment group, sex, weight, and age. One-way ANOVA followed by Dunnett's multiple comparisons test was used to compare MFAP4 and integrin expression in vehicle-, hAS0326-, or ranibizumab-treated groups at a single time point (week 22) relative to control group.

hAS0326 half-life analysis was performed using either one- or two-phase decay according to distribution of data.

p values of 0.05 and below were considered statistically significant.

Study approvals

Collection of samples of vitreous from patients with retinal disease was performed after local full ethics committee approval (20-1165_1) in accordance with the European Guidelines for Good Clinical Practice and the Declaration of Helsinki. Informed consent was obtained from each patient before the collection. The study was approved the local Ethics Committee of University of Heidelberg. Written informed consent was obtained from all patients and the study was conducted in accordance with the Helsinki Declaration.

Regarding patient eye samples used for immunohistochemistry, the study was approved by the Regional Committee on Health Research Ethics for the Capital Region of Denmark (H-23068826). The study was conducted in accordance with the Helsinki Declaration.

Postmortem donor eye tissue was recovered by VisionGift (Portland, OR, USA) and processed in tissue banks where the donated tissue was de-identified (FEI: 3001239138). The tissue was recovered with the authorization for research use by the legal next of kin.

Animal studies

All treatment of animals conformed to the Association for Research in Vision and Ophthalmology (ARVO) Statement for the Use of Animals in Ophthalmic and Vision Research. The rat tolerability study was approved by the University of Oklahoma Health Science Center's Institutional Animal Care and Use Committee. Mouse CNV model, rat STZ model, and injection of antibody into rabbit eyes were performed in compliance with University of Nottingham institutional guidelines and under a UK Home Office license at the University of Nottingham Biological Services Unit (30/3184). Adult African green monkeys were collected and studied at Virscio located on the St. Kitts Biomedical Research Foundation campus, Lower Bourryeau Estate, St. Kitts, West Indies. All work was conducted with the prior approval of the Institutional Animal Care and Use Committee of that facility.

DATA AND CODE AVAILABILITY

The crystallography coordinates and diffraction data of MFAP4 interaction with hAS0326 Fab are deposited in the protein databank as entry 7ZMK. The mass spectrometry proteomics data have been uploaded as supplemetary files.

ACKNOWLEDGMENTS

We thank Lions VisionGift, Portland, OR, for providing samples of human eyes. We thank chief operating officer, EyeCRO LLC, OK Rafal Farjo for the execution of ophthalmic toxicology of hAS0326 in rat eyes. We further thank technicians Vicki Nielsen and Tine Drud Lüttge Rasmussen for experimental assistance.

The study has received funding from Novo Nordisk Foundation Exploratory pre-seed grant (U.H. and G.L.S.), SDU Proof-of-Concept grant (U.H. and G.L.S.), Novo Nordisk Foundation Pre-Seed grant (U.H. and G.L.S.), Bayer Healthcare – Grants4Targets (UH, 2015-08-1388), Novo Nordisk Foundation – Project grant in endocrinology (G.L.S., NNF17OC0026790 and NNF16OC0021136), Øjenforeningen Fight for Sight Denmark (G.L.S. and B.P.), Odense University Hospital Research Fund (J.G. and G.L.S.), Innovation Fund Denmark – Grand Solutions (G.L.S., 7076-00008B), Synoptikfonden (B.P.), C. C. Klestrup og hustru Henriette Klestrups Mindelegat (B.P.), Familien Hede Nielsens Fond (B.P.), Torben og Alice Frimodts Fond (B.P.), Skibsreder Per Henriksen, R. og hustrus Fond (B.P.), Ingeniør K. A. Rohde og Hustrus Legat (B.P.), Augustinus Fonden (B.P.), Fabrikant Jørgen Møllers Mindefond (B.P.), Brødrene Hartmanns Fond (B.P.), Eva og Hans Carl Holms Mindelegat (B.P.), Fonden til Lægevidenskabens Fremme (B.P.), Fabrikant Einar Willumsens Mindelegat (B.P.), Ingeniør August Frederik Wedell Erichsens Legat (BP), Grosserer Christian Andersen og hustru Ingeborg Ovidia Signe Andersen, født Schmidts Legat (B.P.), Odense University Hospital (Forskningspulje mellem RH og OUH) (G.L.S. and S.H.), and Hørslev Fonden (G.L.S.).

AUTHOR CONTRIBUTIONS

Conceptualization, A.S., U.H., and G.L.S.; methodology and investigations, A.S., B.P., C.A., A.V.B., A.P.L., J.H., N.V., Z.B., D.H., S.S., M.O., S.M., I.D., M.K., H.C.B., L.B.S., W.H., N.S.L., B.I., C.L., and H.A.; study design, A.S., B.P., T.L.A., J.H.G., S.H., G.R.A., W.H., M.S.L., J.G., U.H., D.O.B., and G.L.S.; writing – original draft, A.S., B.P., and G.L.S.; project administration, G.L.S.; funding acquisition, U.H., G.L.S., B.P., J.G., and S.H. All authors revised and approved the manuscript.

DECLARATION OF INTERESTS

A.S., U.H., and G.L.S are inventors on US Patent No. 9,988,442 and EP17199552.5 owned by University of Southern Denmark. D.O.B. is inventor on patents, shareholder, employee, and board member in Exonate Ltd. C.A. is an employee at Exonate Ltd. Exonate is a biopharmaceutical company focused on the discovery and development of small-molecule drugs targeting pathological blood vessel formation (angiogenesis) in ophthalmic conditions.

DECLARATION OF GENERATIVE AI AND AI-ASSISTED TECHNOLOGIES IN THE WRITING PROCESS

During the preparation of this work the authors used ChatGPT in order to check grammar and syntax of selected sentences. After using this tool, the authors reviewed and edited the content as needed and take full responsibility for the content of the publication.

SUPPLEMENTAL INFORMATION

Supplemental information can be found online at https://doi.org/10.1016/j.ymthe.2025.01.038.

REFERENCES

1. Sedeh, F.B., Scott, D.A.R., Subhi, Y., and Sørensen, T.L. (2017). Prevalence of neovascular age-related macular degeneration and geographic atrophy in Denmark. Dan. Med. J. *64*, A5422.
2. Ogurtsova, K., da Rocha Fernandes, J.D., Huang, Y., Linnenkamp, U., Guariguata, L., Cho, N.H., Cavan, D., Shaw, J.E., and Makaroff, L.E. (2017). IDF Diabetes Atlas: Global estimates for the prevalence of diabetes for 2015 and 2040. Diabetes Res. Clin. Pract. *128*, 40–50.
3. Yau, J.W.Y., Rogers, S.L., Kawasaki, R., Lamoureux, E.L., Kowalski, J.W., Bek, T., Chen, S.J., Dekker, J.M., Fletcher, A., Grauslund, J., et al. (2012). Global prevalence and major risk factors of diabetic retinopathy. Diabetes Care *35*, 556–564.
4. Chandra, S., Arpa, C., Menon, D., Khalid, H., Hamilton, R., Nicholson, L., Pal, B., Fasolo, S., Hykin, P., Keane, P.A., and Sivaprasad, S. (2020). Ten-year outcomes of antivascular endothelial growth factor therapy in neovascular age-related macular degeneration. Eye (Lond) *34*, 1888–1896.
5. Bhatwadekar, A.D., Kansara, V., Luo, Q., and Ciulla, T. (2020). Anti-integrin therapy for retinovascular diseases. Expert Opin. Investig. Drugs *29*, 935–945.
6. Friedlander, M., Theesfeld, C.L., Sugita, M., Fruttiger, M., Thomas, M.A., Chang, S., and Cheresh, D.A. (1996). Involvement of integrins alpha v beta 3 and alpha v beta 5 in ocular neovascular diseases. Proc. Natl. Acad. Sci. USA *93*, 9764–9769.
7. Wilkinson-Berka, J.L., Jones, D., Taylor, G., Jaworski, K., Kelly, D.J., Ludbrook, S.B., Willette, R.N., Kumar, S., and Gilbert, R.E. (2006). SB-267268, a nonpeptidic antagonist of alpha(v)beta3 and alpha(v)beta5 integrins, reduces angiogenesis and VEGF expression in a mouse model of retinopathy of prematurity. Invest. Ophthalmol. Vis. Sci. *47*, 1600–1605.
8. Tsou, R., and Isik, F.F. (2001). Integrin activation is required for VEGF and FGF receptor protein presence on human microvascular endothelial cells. Mol. Cell. Biochem. *224*, 81–89.
9. Pilecki, B., Holm, A.T., Schlosser, A., Moeller, J.B., Wohl, A.P., Zuk, A.V., Heumüller, S.E., Wallis, R., Moestrup, S.K., Sengle, G., et al. (2016). Characterization of Microfibrillar-associated Protein 4 (MFAP4) as a Tropoelastin- and Fibrillin-binding Protein Involved in Elastic Fiber Formation. J. Biol. Chem. *291*, 1103–1114.
10. Schlosser, A., Pilecki, B., Hemstra, L.E., Kejling, K., Kristmannsdottir, G.B., Wulf-Johansson, H., Moeller, J.B., Füchtbauer, E.M., Nielsen, O., Kirketerp-Møller, K., et al. (2016). MFAP4 Promotes Vascular Smooth Muscle Migration, Proliferation and Accelerates Neointima Formation. Arterioscler. Thromb. Vasc. Biol. *36*, 122–133.
11. Pilecki, B., Schlosser, A., Wulf-Johansson, H., Trian, T., Moeller, J.B., Marcussen, N., Aguilar-Pimentel, J.A., de Angelis, M.H., Vestbo, J., Berger, P., et al. (2015). Microfibrillar-associated protein 4 modulates airway smooth muscle cell phenotype in experimental asthma. Thorax *70*, 862–872.
12. Wulf-Johansson, H., Lock Johansson, S., Schlosser, A., Trommelholt Holm, A., Rasmussen, L.M., Mickley, H., Diederichsen, A.C.P., Munkholm, H., Poulsen, T.S.,

Tornøe, I., et al. (2013). Localization of Microfibrillar-Associated Protein 4 (MFAP4) in Human Tissues: Clinical Evaluation of Serum MFAP4 and Its Association with Various Cardiovascular Conditions. PLoS One *8*, e82243.

13. Pilecki, B., de Carvalho, P.V.S.D., Kirketerp-Møller, K.L., Schlosser, A., Kejling, K., Dubik, M., Madsen, N.P., Stubbe, J., Hansen, P.B.L., Andersen, T.L., et al. (2021). MFAP4 Deficiency Attenuates Angiotensin II-Induced Abdominal Aortic Aneurysm Formation Through Regulation of Macrophage Infiltration and Activity. Front. Cardiovasc. Med. *8*, 764337.

14. Christensen, K.B., Unsal, S., Ebbesen, M.F., Hemstra, L., Schlosser, A., Rosenstand, K., Hansen, P.B.L., Jensen, B.L., Bloksgaard, M., Simonsen, U., et al. (2024). MFAP4-Deficiency Aggravates Age-Induced Changes in Resistance Artery Structure, While Ameliorating Hypertension. Hypertension *81*, 1308–1319. https://doi.org/10.1161/HYPERTENSIONAHA.123.22283.

15. Saekmose, S.G., Schlosser, A., Holst, R., Johansson, S.L., Wulf-Johansson, H., Tornoe, I., Vestbo, J., Kyvik, K.O., Barington, T., Holmskov, U., et al. (2013). Enzyme-linked immunosorbent assay characterization of basal variation and heritability of systemic microfibrillar-associated protein 4. PLoS One *8*, e82383.

16. Hsiao, C.T., Cheng, H.W., Huang, C.M., Li, H.R., Ou, M.H., Huang, J.R., Khoo, K.H., Yu, H.W., Chen, Y.Q., Wang, Y.K., et al. (2017). Fibronectin in cell adhesion and migration via N-glycosylation. Oncotarget *8*, 70653–70668.

17. Mitchell, P., Liew, G., Gopinath, B., and Wong, T.Y. (2018). Age-related macular degeneration. Lancet *392*, 1147–1159.

18. Shrive, A.K., Moeller, J.B., Burns, I., Paterson, J.M., Shaw, A.J., Schlosser, A., Sorensen, G.L., Greenhough, T.J., and Holmskov, U. (2014). Crystal structure of the tetrameric fibrinogen-like recognition domain of fibrinogen C domain containing 1 (FIBCD1) protein. J. Biol. Chem. *289*, 2880–2887.

19. Su, G., Atakilit, A., Li, J.T., Wu, N., Bhattacharya, M., Zhu, J., Shieh, J.E., Li, E., Chen, R., Sun, S., et al. (2012). Absence of integrin alphavbeta3 enhances vascular leak in mice by inhibiting endothelial cortical actin formation. Am. J. Respir. Crit. Care Med. *185*, 58–66.

20. Pulous, F.E., and Petrich, B.G. (2019). Integrin-dependent regulation of the endothelial barrier. Tissue Barriers *7*, 1685844.

21. Aman, J., and Margadant, C. (2023). Integrin-Dependent Cell-Matrix Adhesion in Endothelial Health and Disease. Circ. Res. *132*, 355–378.

22. Patel, C., Goody, R., Hu, W., Kurian, A., James, D., Torres, R., Christie, L.A., Hohman, T., and Lawrence, M. (2020). Primate model of chronic retinal neovascularization and vascular leakage. Exp. Eye Res. *195*, 108031.

23. Zhang, Q., Yan, X., Han, H., Wang, Y., and Sun, J. (2024). Pericyte in retinal vascular diseases: A multifunctional regulator and potential therapeutic target. FASEB J. *38*, e23679.

24. Puebla, M., Tapia, P.J., and Espinoza, H. (2022). Key Role of Astrocytes in Postnatal Brain and Retinal Angiogenesis. Int. J. Mol. Sci. *23*, 2646.

25. Li, X., Liu, J., Hoh, J., and Liu, J. (2019). Muller cells in pathological retinal angiogenesis. Transl. Res. *207*, 96–106.

26. Wang, H.B., Yang, J., Shuai, W., Yang, J., Liu, L.B., Xu, M., and Tang, Q.Z. (2020). Deletion of Microfibrillar-Associated Protein 4 Attenuates Left Ventricular Remodeling and Dysfunction in Heart Failure. J. Am. Heart Assoc. *9*, e015307.

27. Pan, Z., Yang, K., Wang, H., Xiao, Y., Zhang, M., Yu, X., Xu, T., Bai, T., and Zhu, H. (2020). MFAP4 deficiency alleviates renal fibrosis through inhibition of NF-kappaB and TGF-beta/Smad signaling pathways. FASEB J. *34*, 14250–14263.

28. Abrahamsen, L., Blindbæk, S.L., Schlosser, A., Koss, M., Dacheva, I., Lind, M., Holmskov, U., Sørensen, G.L., and Grauslund, J. (2017). Intraocular expression of microfibrillar-associated protein 4 (MFAP4) in patients with neovascular age-related macular degeneration (nAMD). Acta ophthalmologica *95*. Abstract. https://doi.org/10.1111/j.1755-3768.2017.0F049.

29. Van Hove, I., Hu, T.T., Beets, K., Van Bergen, T., Etienne, I., Stitt, A.W., Vermassen, E., and Feyen, J.H.M. (2021). Targeting RGD-binding integrins as an integrative therapy for diabetic retinopathy and neovascular age-related macular degeneration. Prog. Retin. Eye Res. *85*, 100966.

30. Wozny, M.R., Nelea, V., Siddiqui, I.F.S., Wanga, S., de Waard, V., Strauss, M., and Reinhardt, D.P. (2024). Microfibril-associated glycoprotein 4 forms octamers that mediate interactions with elastogenic proteins and cells. Nat. Commun. *15*, 4015.

31. Cheresh, D.A., and Stupack, D.G. (2008). Regulation of angiogenesis: apoptotic cues from the ECM. Oncogene *27*, 6285–6298.

32. Chen, X.L., Nam, J.O., Jean, C., Lawson, C., Walsh, C.T., Goka, E., Lim, S.T., Tomar, A., Tancioni, I., Uryu, S., et al. (2012). VEGF-induced vascular permeability is mediated by FAK. Dev. Cell *22*, 146–157.

33. Li, Y., Busoy, J.M., Zaman, B.A.A., Tan, Q.S.W., Tan, G.S.W., Barathi, V.A., Cheung, N., Wei, J.J.Y., Hunziker, W., Hong, W., et al. (2018). A novel model of persistent retinal neovascularization for the development of sustained anti-VEGF therapies. Exp. Eye Res. *174*, 98–106.

34. Young, K.A., Biggins, L., and Sharpe, H.J. (2021). Protein tyrosine phosphatases in cell adhesion. Biochem. J. *478*, 1061–1083.

35. Hermann, M.R., Jakobson, M., Colo, G.P., Rognoni, E., Jakobson, M., Kupatt, C., Posern, G., and Fässler, R. (2016). Integrins synergise to induce expression of the MRTF-A-SRF target gene ISG15 for promoting cancer cell invasion. J. Cell Sci. *129*, 1391–1403.

36. Krzystolik, M.G., Afshari, M.A., Adamis, A.P., Gaudreault, J., Gragoudas, E.S., Michaud, N.A., Li, W., Connolly, E., O'Neill, C.A., and Miller, J.W. (2002). Prevention of experimental choroidal neovascularization with intravitreal anti-vascular endothelial growth factor antibody fragment. Arch. Ophthalmol. *120*, 338–346.

37. Surowka, M., Schaefer, W., and Klein, C. (2021). Ten years in the making: application of CrossMab technology for the development of therapeutic bispecific antibodies and antibody fusion proteins. MAbs *13*, 1967714.

38. Humphries, J.D., Byron, A., and Humphries, M.J. (2006). Integrin ligands at a glance. J. Cell Sci. *119*, 3901–3903.

39. Bachmann, M., Schafer, M., Mykuliak, V.V., Ripamonti, M., Heiser, L., Weissenbruch, K., Krubel, S., Franz, C.M., Hytonen, V.P., Wehrle-Haller, B., et al. (2020). Induction of ligand promiscuity of alphaVbeta3 integrin by mechanical force. J. Cell Sci *11*, jcs242404.

40. Kuppermann, B.D. (2015). A dual-mechanism drug for vitreoretinal diseases. https://retinatoday.com/articles/2015-july-aug/a-dual-mechanism-drug-for-vitreoretinal-diseases.

41. Gonzalez, V. (2016). The Promise of Integrin Receptors for Treating Vitreoretinal Disorders. https://retinatoday.com/articles/2016-july-aug/the-promise-of-integrin-receptors-for-treating-vitreoretinal-disorders.

42. Dugel, P.U. (2019). The Scoop on Anti-Integrin Therapy for DME. https://retinatoday.com/articles/2019-jan-feb/the-scoop-on-anti-integrin-therapy-for-dme.

43. Askew, B.C., Furuya, T., and Edwards, D.S. (2018). Ocular Distribution and Pharmacodynamics of SF0166, a Topically Administered alphavbeta3 Integrin Antagonist, for the Treatment of Retinal Diseases. J. Pharmacol. Exp. Ther. *366*, 244–250.

44. Lapoce, C. (2024). Ophthalmology Month in Review: March 2024. https://www.hcplive.com/view/ophthalmology-month-in-review-march-2024.

45. Voigt, A.P., Whitmore, S.S., Lessing, N.D., DeLuca, A.P., Tucker, B.A., Stone, E.M., Mullins, R.F., and Scheetz, T.E. (2020). Spectacle: An interactive resource for ocular single-cell RNA sequencing data analysis. Exp. Eye Res. *200*, 108204.

46. Voigt, A.P., Binkley, E., Flamme-Wiese, M.J., Zeng, S., DeLuca, A.P., Scheetz, T.E., Tucker, B.A., Mullins, R.F., and Stone, E.M. (2020). Single-Cell RNA Sequencing in Human Retinal Degeneration Reveals Distinct Glial Cell Populations. Cells *9*, 438.

47. Voigt, A.P., Whitmore, S.S., Mulfaul, K., Chirco, K.R., Giacalone, J.C., Flamme-Wiese, M.J., Stockman, A., Stone, E.M., Tucker, B.A., Scheetz, T.E., and Mullins, R.F. (2020). Bulk and single-cell gene expression analyses reveal aging human choriocapillaris has pro-inflammatory phenotype. Microvasc. Res. *131*, 104031.

48. Voigt, A.P., Mulfaul, K., Mullin, N.K., Flamme-Wiese, M.J., Giacalone, J.C., Stone, E.M., Tucker, B.A., Scheetz, T.E., and Mullins, R.F. (2019). Single-cell transcriptomics of the human retinal pigment epithelium and choroid in health and macular degeneration. Proc. Natl. Acad. Sci. USA *116*, 24100–24107.

49. Voigt, A.P., Whitmore, S.S., Flamme-Wiese, M.J., Riker, M.J., Wiley, L.A., Tucker, B.A., Stone, E.M., Mullins, R.F., and Scheetz, T.E. (2019). Molecular characterization of foveal versus peripheral human retina by single-cell RNA sequencing. Exp. Eye Res. *184*, 234–242.

50. Koss, M.J., Pfister, M., Rothweiler, F., Michaelis, M., Cinatl, J., Schubert, R., and Koch, F.H. (2012). Comparison of cytokine levels from undiluted vitreous of untreated patients with retinal vein occlusion. Acta Ophthalmol. *90*, e98–e103.

51. Wilkinson, C.P., Ferris, F.L., 3rd, Klein, R.E., Lee, P.P., Agardh, C.D., Davis, M., Dills, D., Kampik, A., Pararajasegaram, R., and Verdaguer, J.T.; Global Diabetic Retinopathy Project Group (2003). Proposed international clinical diabetic retinopathy and diabetic macular edema disease severity scales. Ophthalmology *110*, 1677–1682.

52. Lassen, N.E., Andersen, T.L., Pløen, G.G., Søe, K., Hauge, E.M., Harving, S., Eschen, G.E.T., and Delaisse, J.M. (2017). Coupling of Bone Resorption and Formation in Real Time: New Knowledge Gained From Human Haversian BMUs. J. Bone Miner. Res. *32*, 1395–1405.

53. Schlosser, A., Thomsen, T., Shipley, J.M., Hein, P.W., Brasch, F., Tornøe, I., Nielsen, O., Skjødt, K., Palaniyar, N., Steinhilber, W., et al. (2006). Microfibril-associated protein 4 binds to surfactant protein A (SP-A) and colocalizes with SP-A in the extracellular matrix of the lung. Scand. J. Immunol. *64*, 104–116.

54. Lausen, M., Lynch, N., Schlosser, A., Tornoe, I., Saekmose, S.G., Teisner, B., Willis, A.C., Crouch, E., Schwaeble, W., and Holmskov, U. (1999). Microfibril-associated protein 4 is present in lung washings and binds to the collagen region of lung surfactant protein D. J. Biol. Chem. *274*, 32234–32240.

55. Kabsch, W. (2010). Integration, scaling, space-group assignment and post-refinement. Acta Crystallogr. D Biol. Crystallogr. *66*, 133–144.

56. McCoy, A.J., Grosse-Kunstleve, R.W., Adams, P.D., Winn, M.D., Storoni, L.C., and Read, R.J. (2007). Phaser crystallographic software. J. Appl. Crystallogr. *40*, 658–674.

57. Afonine, P.V., Grosse-Kunstleve, R.W., Echols, N., Headd, J.J., Moriarty, N.W., Mustyakimov, M., Terwilliger, T.C., Urzhumtsev, A., Zwart, P.H., and Adams, P.D. (2012). Towards automated crystallographic structure refinement with phenix.refine. Acta Crystallogr. D Biol. Crystallogr. *68*, 352–367.

58. Croll, T.I., and Andersen, G.R. (2016). Re-evaluation of low-resolution crystal structures via interactive molecular-dynamics flexible fitting (iMDFF): a case study in complement C4. Acta Crystallogr. D Struct. Biol. *72*, 1006–1016.

59. Chen, V.B., Arendall, W.B., 3rd, Headd, J.J., Keedy, D.A., Immormino, R.M., Kapral, G.J., Murray, L.W., Richardson, J.S., and Richardson, D.C. (2010). MolProbity: all-atom structure validation for macromolecular crystallography. Acta Crystallogr. D Biol. Crystallogr. *66*, 12–21.

60. Schrodinger, L. (2015). The PyMOL Molecular Graphics System. Version 1.8.

61. Krissinel, E., and Henrick, K. (2007). Inference of macromolecular assemblies from crystalline state. J. Mol. Biol. *372*, 774–797.

62. Green, K.R., Beazley-Long, N., Lynch, A.P., Allen, C.L., Bates, D.O., and Benest, A.V. (2022). Quantification of Angiogenesis in Laser Choroidal Neovascularization. Methods Mol. Biol. *2441*, 223–231.

63. Malhi, N.K., Bates, D.O., Arkill, K.P., and Allen, C.L. (2022). Noninvasive Measurement of Retinal Microvascular Permeability During Loss of Endothelial Quiescence. Methods Mol. Biol. *2441*, 135–156.

64. Kiss, S., Oresic Bender, K., Grishanin, R.N., Hanna, K.M., Nieves, J.D., Sharma, P., Nguyen, A.T., Rosario, R.J., Greengard, J.S., Gelfman, C.M., and Gasmi, M. (2021). Long-Term Safety Evaluation of Continuous Intraocular Delivery of Aflibercept by the Intravitreal Gene Therapy Candidate ADVM-022 in Nonhuman Primates. Transl. Vis. Sci. Technol. *10*, 34.

65. Wu, T., Hu, E., Xu, S., Chen, M., Guo, P., Dai, Z., Feng, T., Zhou, L., Tang, W., Zhan, L., et al. (2021). ClusterProfiler 4.0: A universal enrichment tool for interpreting omics data. Innovation. *2*, 100141.